NASA/CR–2017-219636

Lift Recovery for AFC-Enabled High Lift System

Arvin Shmilovich, Yoram Yadlin, and Eric D. Dickey
The Boeing Company, Huntington Beach, California

Abraham N. Gissen and Edward A. Whalen
The Boeing Company, St. Louis, Missouri

July 2017

NASA STI Program . . . in Profile

Since its founding, NASA has been dedicated to the advancement of aeronautics and space science. The NASA scientific and technical information (STI) program plays a key part in helping NASA maintain this important role.

The NASA STI program operates under the auspices of the Agency Chief Information Officer. It collects, organizes, provides for archiving, and disseminates NASA's STI. The NASA STI program provides access to the NTRS Registered and its public interface, the NASA Technical Reports Server, thus providing one of the largest collections of aeronautical and space science STI in the world. Results are published in both non-NASA channels and by NASA in the NASA STI Report Series, which includes the following report types:

- TECHNICAL PUBLICATION. Reports of completed research or a major significant phase of research that present the results of NASA Programs and include extensive data or theoretical analysis. Includes compilations of significant scientific and technical data and information deemed to be of continuing reference value. NASA counter-part of peer-reviewed formal professional papers but has less stringent limitations on manuscript length and extent of graphic presentations.

- TECHNICAL MEMORANDUM. Scientific and technical findings that are preliminary or of specialized interest, e.g., quick release reports, working papers, and bibliographies that contain minimal annotation. Does not contain extensive analysis.

- CONTRACTOR REPORT. Scientific and technical findings by NASA-sponsored contractors and grantees.

- CONFERENCE PUBLICATION. Collected papers from scientific and technical conferences, symposia, seminars, or other meetings sponsored or co-sponsored by NASA.

- SPECIAL PUBLICATION. Scientific, technical, or historical information from NASA programs, projects, and missions, often concerned with subjects having substantial public interest.

- TECHNICAL TRANSLATION. English-language translations of foreign scientific and technical material pertinent to NASA's mission.

Specialized services also include organizing and publishing research results, distributing specialized research announcements and feeds, providing information desk and personal search support, and enabling data exchange services.

For more information about the NASA STI program, see the following:

- Access the NASA STI program home page at http://www.sti.nasa.gov

- E-mail your question to help@sti.nasa.gov

- Phone the NASA STI Information Desk at 757-864-9658

- Write to:
  NASA STI Information Desk
  Mail Stop 148
  NASA Langley Research Center
  Hampton, VA 23681-2199

NASA/CR–2017-219636

Lift Recovery for AFC-Enabled High Lift System

Arvin Shmilovich, Yoram Yadlin, and Eric D. Dickey
The Boeing Company, Huntington Beach, California

Abraham N. Gissen and Edward A. Whalen
The Boeing Company, St. Louis, Missouri

National Aeronautics and
Space Administration

Langley Research Center
Hampton, Virginia 23681-2199

Prepared for Langley Research Center
under Contract NNL16AB02T

July 2017

Acknowledgments

This study was carried out under NASA Contract: NNL16AB02T/NNL16AA04B. Dr. John C. Lin was the NASA LaRC Task Principal Investigator. In addition to the authors, the following Boeing personnel contributed to this work: Paul M. Vijgen, Douglas S. Lacy.

TABLE OF CONTENTS

1. Background and Previous Work

1.1 Introduction

Boeing has evaluated candidate Active Flow Control (AFC) concepts for meeting high-lift requirements for takeoff and landing of a transonic transport aircraft configuration with a simplified high-lift system.

This project is a continuation of the NASA AFC-Enabled Simplified High-Lift System Integration Study contract (NNL10AA05B) performed by Boeing under the Fixed Wing Project. This task is motivated by the simplified high-lift system, which is advantageous due to the simpler mechanical system, reduced actuation power and lower maintenance costs. Additionally, the removal of the flap track fairings associated with conventional high-lift systems renders a more efficient aerodynamic configuration. Potentially, these benefits translate to a ~2.25% net reduction in fuel burn for a twin-engine, long-range airplane.

In Phase I (AFC-Enabled Simplified High-Lift System Integration Study, Contract/Task Order NNL10AA05B/NNL13AB65T) Boeing demonstrated computationally that flow control applied to a high-lift configuration that consists of simple hinge flaps is capable of attaining the performance of a conventional counterpart. In this study, only actuation methods that require an air supply have been considered since they are especially effective for high-lift applications. However, in this initial implementation, the mass flow required for actuation was excessive, rendering it impractical. The initial conventional high-lift airplane configuration was derived from the Common Research Model (CRM) cruise geometry and it is designated HL-CRM-1 (High-Lift CRM-1). These results are documented in Reference 1.

In Phase II (Refined AFC-Enabled High-Lift System Integration Study, Contract/Task Order NNL10AA05B/NNL14AB98T), Boeing developed a more efficient flow control technique that is based on the traverse actuation[2]. Computational evaluations indicate that this solution offers a substantial reduction in required mass flow, less than one tenth of the mass flow estimate from Phase I. More importantly, the mass flow required for traversing actuation falls within available resources onboard a commercial aircaft. Although these findings provide added motivation in the search for practical simplified high-lift systems, it is noted that the integration of the new actuation method hinges upon a successful implementation of a traverse actuator. This study is described in Reference 3.

A summary of main results obtained under this contract (Phases I and II) is shown in Figures 1.1. It presents the airplane lift increment due to various modes of actuation on the simplified configurations at the nominal landing condition of $\alpha=8^{o}$. HL-CRM-1 produces a lift coefficient of 1.66 and it represents the target lift level for the AFC system. The curves represent a collection of AFC techniques in pursuit of a solution with respect to practical mass flow rates. Starting from the initial case (black curve) and marching leftwards the curves represent a time line of the progress made in the course of this study.

The initial AFC implementation in Phase I, which was based on a set of discrete convergent/divergent (CD) ducts resulted in an exorbitant fluidic supply requirement (black curve). Substituting the ducts with an array of fluidic oscillators resulted in a rather meager 10% reduction in mass flow (dashed black line).

In Phase II, subsequent refinements of the AFC construct using a set of convergent/divergent ducts helped reduce the required mass flow by more than 50%, but a substantial air supply was still required (blue curve). The next implementation, which consists of a continuous convergent-divergent duct spanning the length of the inboard flap, was shown to further lower the required mass flow (green). However, only the traverse actuation modes help to reduce the input to within practical levels (red symbols). The traverse actuation is applied on the inboard flap as described in Figure 1.2. It consists of a high velocity jet packet that travels periodically along the span of the flap close to the hinge line, in a crabwise motion. Traverse actuation is especially effective when the frequency of actuation is consistent with the characteristic time scale of the flow. Figure 1.3 shows the computed flow fields of HL-CRM-1, the simplified high-lift configuration and the AFC-enabled system with one of the traverse actuation

modes. The crossflow motion due to the traverse actuation produces momentary flow attachment in the region around the respective wing section. The continuous actuation results in improved streamlining of the flow at the flap in a time-average sense. It also creates an induced ripple effect that helps attach the flow over the outboard wing segment. The combined effects increase global circulation, which results in greater lift production as seen from the surface pressure distributions. Details of the computational study and the step-by-step process leading to the AFC solution are described in Reference 4.

Separately and outside of this contract Boeing has developed an improved conventional high-lift configuration, also based on the CRM cruise geometry, dubbed HL-CRM (Reference 5). In the current Request for Proposal, NASA seeks to further explore innovative flow control concepts in conjunction with a simple hinge flap system that will provide high-lift performance comparable to HL-CRM (see Figure 1.1). Clearly this represents a more ambitious objective since AFC has to recover a larger lift shortfall of the simplified high-lift system.

1.2. Scope and Objectives

In the current project (Phase III) Boeing focuses on the development of candidate AFC approaches for a simplified high-lift system that meets the performance of HL-CRM. To achieve this, Boeing will employ a proprietary technique based on the traverse actuation[6,7]. While the actuation approach is considered proprietary, the data generated under this contract will be provided with unlimited rights. This investigation is viewed as a risk reduction step ahead of the design and fabrication of a wind tunnel model with an AFC-enabled high-lift system, which will lead to the experimental confirmation of the most promising AFC concept. The same guidelines and requirements used in the prior phases are adopted in this investigation. The key requirement is that the mass flow for actuation and the supply pressure have to be within available resources onboard (e.g., commensurate with supply of Auxiliary Power Units or within engine bleed limits).

1.3. Approach

Computational simulations are used to guide the development of the flow control implementations. This investigation draws heavily on the lessons learned during the earlier phases described in Section 1.1. Although the focus is on identifying promising AFC methods using CFD analysis, general aspects of airplane integration are also considered while developing actuation methods and AFC layouts. Design aspects of the integration (e.g., pressure, mass flow and manufacturability) of the AFC method into a subscale model for wind tunnel demonstrations at the NASA 14x22 ft wind tunnel are also considered.

AFC simulations are performed for the simplified takeoff and landing configurations and the performance is gauged against HL-CRM at the nominal landing condition. The objective is to match the lift of the conventional system. The AFC system should require mass flow comparable to the level achieved in Phase II, or lower.

1.4. Description of Tasks to be Performed

The investigation employs a two-step strategy. First a simplified high-lift configuration has been developed, similar to the process used in the earlier Phase II. The analysis employs a large flap deflection and onger flap chord size for enhanced efficiency of flow control while staying clear of the model wing spars. The second step of the study focuses on computational assessment of a set of AFC implementations. The traverse actuation technique, which was found to be very effective in Phase II, is utilized for achieving design objectives. Boeing has also investigated more effective traverse actuation variants and actuation techniques. These methods have been independently developed by Boeing.

Aspects of implementation for ease of integration are generally considered. Actuator parts need to be large enough (e.g., orifice height greater than 0.01") to accommodate manufacturing and integration into a 10%-scale model. Mass flow rates and pressure levels are continuously assessed for feasibility.

This report includes CFD simulation results and assessments of the recommended solution for the AFC-enabled high-lift configuration. A set of recommendations are put forth with the focus on elevating the AFC technology readiness and potentially providing a pathway towards future applications.

2. Baseline Geometry

In order to meet the higher lift level of HL-CRM, a revised simplified high-lift system is first considered to facilitate more effective AFC implementations. Since flow control is particularly effective in reducing flow separation, configurations that produce sizeable separation in the uncontrolled mode would be suitable candidates. This can be accomplished with higher flap deflection, larger flap chord, or a combination thereof. Relative to the configuration with $\delta_f = 50°$ and nominal flap chord length of $C_f = 1$, two variants will be evaluated here; one with a larger flap deflection of 70° and another with $\delta_f = 50°$ and a 25% longer flap chord.

2.1 Configuration $\delta_f = 70°$, $C_f = 1$

Based on the current convention, the inboard (IB) flap is deflected to 70° and the outboard (OB) flap segment is deflected accordingly in order to create a continuous flap surface in the span direction. In other words, there is no flow through the outer edge of the IB flap and the inboard edge of the OB flap. This configuration is depicted in Figure 2.1.

The flow control analyses incorporate the spanwise convergent/divergent nozzle embedded into the IB flap. It consists of a two-dimensional nozzle whose exit section forms a long slot along a backward facing step (described in Section V-B-4 in Reference 4). Constant blowing is achieved by applying high pressure at the nozzle inlet. In the first set of results the nozzle is placed at the same physical location as in the original $\delta_f = 50°$ configuration. In other words, in both of these configurations the nozzles are at the same distance from the hinge lines. More specifically, this nominal port placement is denoted X1 and it corresponds to the 85.8% chord station at the mid IB flap at y=275". Also, the nozzles are at the same angle relative to the respective local surfaces. The cross sections of the mid IB flap are shown in Figure 2.2 in a sequence of close up views.

The nominal landing condition is considered in this study. This condition corresponds to a free stream Mach number of 0.2, an angle-of-attack of 8° and Reynolds number of 3.3 million based on the mean aerodynamic chord. The baseline and flow control cases for the two flap deflections are shown in Figure 2.3. In the AFC-off case, the higher flap deflection produces a larger separation bubble on both flap elements. Flow control with PR=4.8 (where PR is the pressure ratio) is quite effective in attaching the flow up to the trailing edge at both flap deflections. Interestingly, the separation on the OB flap is larger when flow control is applied with a PR=4.8. This is due to the elevated global circulation as can be inferred from the higher suction of the entire wing. Also, the separation pocket at the side of body is noticeably bigger at the higher flap deflection due to the more pronounced flap edge effect. Nevertheless, when the flow is attached, the larger camber of the 70° flap deflection results in higher lift.

The flow fields over a range of actuation pressure ratios are shown in Figure 2.4. Inlet pressure ratio of 1.6 is only partially effective in attaching the flow. Increasing the input pressure is quite effective in attaching the flow on the IB flap. However, the actuation in the regime of circulation control at PR higher than about 3 is less efficient. Figure 2.5 describes the flow fields at the mid IB flap section for selected actuation levels. Here flow separation is defined as the regions of flow reversal based on the streamwise component of the velocity vector. It illustrates the Coanda effect at the high PR levels as a result of the high velocity jets that adhere to the surface over a large distance.

Figure 2.6 shows the lift gains due to the actuation at X1 for the different flap deflections. The target lift is achievable with the flap deflected at 70° with a reduction of approximately 17% in mass flow relative to the 50° case and at lower PR of 4.0.

The sensitivity to nozzle placement in conjunction with the larger flap deflection is considered next. Two nozzle locations are considered. The first location, denoted X0, is upstream of the nominal location X1, but downstream of the hinge line. X0 corresponds to the 84% chord station at the mid IB flap (which is 3.14" upstream of X1). The second nozzle location is downstream of X1. It is denoted X2 and it is at the 89% chord station of the mid IB flap (3.35" from X1). In all three nozzle locations, the nozzle is placed at approximately the same angle to the respective local surfaces. The cross sectional layouts are shown in Figure 2.7. The nozzle exit stations for the respective locations are indicated with a solid line. For reference, the dashed lines indicate the other nozzle locations.

The cross-sectional flow fields are shown in Figures 2.8 and 2.9 for the AFC-off and AFC-on cases, respectively. In the absence of flow control, the flap is essentially separated over the entire flap. In all the three nozzle systems, the separation originates close to the 85.8% chord station, irrespective of the nozzle location. This station coincides with the nominal nozzle location X1. At this IB flap section, the actuation of PR=4.8 is effective in attaching the flow over its entire length for all nozzle locations. The wing flow fields are shown in Figure 2.10 indicating that the nozzle placement at the downstream location X2 is less effective at the inboard edge of the flap in the side of body region. This is commensurate with the relatively smaller lift increments in Figure 2.11 obtained with the actuation at X2. The results obtained with constant blowing indicate that proper nozzle placement is upstream and close to the separation point (in the X0 to X1 range).

2.2 Configuration $\delta_f = 50°$, $C_f = 1.25$

A 25% longer flap chord is considered next with a deflection of 50°. This system is shown in Figure 2.12 together with the configurations that have been previously analyzed. The nozzle layout at the mid IB flap section is presented in Figure 2.13. In the longer flap, the distance of the nozzle from the hinge line is similar to the respective distances (nozzle-to-hinge) of the nominal location X1 in the other referenced configurations. The nozzles in the three configurations are at the same angle with respect to the local surface. The baseline and the actuated flow fields for the various simplified configurations (with the X1 nozzle location) are shown in Figures 2.14 and 2.15. The baseline flow for the larger flap system results in a noticeably bigger separation region. The actuation with PR=4.8 helps attach the flow in all cases. The cross sectional flow fields in Figure 2.15 illustrate that even in the PR=3.2 case the actuation provides enough momentum to prevent flow separation over the entire flap. Not surprisingly, the flow control is very effective in reducing flow separation on the longer flap case as can be inferred from the lift curve in Figure 2.16. The target lift is achievable with the longer flap deflected at 50° with a reduction in mass flow of approximately 14% relative to the nominal flap size. Also, the target lift is achieved with a low PR of 4.0.

Both of the baseline configurations, the 70° flap deflection and the 25% longer flap, result in reduced actuation input relative to the original geometry. The combined variant of a longer flap size and higher deflection was not evaluated in the current study. It is conceivable that the combined effect of flow control might lead to a cumulative reduction in mass flow in the range of 25-35%. Nevertheless, the original configuration (δ_f=50°, C_f=1) will be used for the remainder of this study in order to systematically evaluate new AFC techniques in relation to solutions obtained during the previous phases of this contract.

3. Thermally Controlled Actuation

Recently and outside of this contract Boeing has developed a method for reduced mass flow required for actuation[8]. It is based on thermal control of the air supply. Specifically, higher air supply temperature results in reduced mass flow. Generally, the aerodynamic benefit from AFC is a function of the momen-

tum coefficient due to actuation. Since the momentum coefficient is not dependent on temperature, the net impact of increased supply temperature results in reduced mass flow with no degradation in AFC performance. More specifically, mass flow is reduced by $\sqrt{T}$, where T is the absolute temperature of the supply. The thermal control concept has been demonstrated computationally for isolated constant blowing actuators, fluidic oscillators and enhanced control authority of a vertical tail. The approach has also been confirmed experimentally on a bench test model of a CD nozzle.

3.1 Whole Hot Supply

The thermal control is applied to the continuous convergent-divergent duct spaning the length of the IB flap. The reduction in mass flow achieved for a set of temperature levels of TR=2 and 4 is illustrated in Figure 3.1a. TR is the ratio of the supply temperature to the free stream temperature. The cold (unheated) supply of TR=1 corresponds to the green curve. The red dash lines connects points of constant PR. Depending on supply temperature, the hot input helps lower the mass flow to the predicted levels, which are proportional to $T^{-1/2}$. However, it is noted that there is slight degradation in lift, especially for the TR=4 case. The lift vs. the actuation momentum coefficient is shown in Figure 3.1b for the various supply temperatures. The collapsing of the curves clearly indicates that the momentum coefficient is the relevant AFC parameter.

Figures 3.2 and 3.3 show the computed flow characteristics with an air supply of PR=3.2 and 6.4, respectively, and temperature levels of TR=1, 2 and 4. The perspective views show the surface pressure and temperature distributions, together with the separated flow regions. The inlet ejection vector, defined by $\rho\mathbf{q}$, is also shown (where ρ is the density and $\mathbf{q}$ is the velocity vector). Note that the vectors progressively get smaller with higher supply temperatures. For these PR values, the nozzle is choked and the inlet velocity is fixed. However, the density is reduced by T^{-1}, therefore the vectors are smaller at higher supply temperatures. The predicted flow fields indicate that the momentum imparted by the actuation helps eliminate the flow separation on nearly the entire span of the IB flap at all supply temperatures. The high temperature actuation is somewhat less effective at the inboard edge of the flap, consistent with the lift curves in Figure 3.1a. This is especially noticable for the PR=6.4 case. The temperature fields indicate localized elevated temperatures on the flap surface in the immediate vicinity of the nozzle.

The cross sectional nozzle flow is described by the Mach number, ρu^2 (momentum), ρu (a measure of mass flow), and temperature. At these high input pressure ratios, the nozzle is choked (the black contour lines represent sonic conditions). For a given PR, the Mach number and the momentum fields are nearly identical with varying inlet temperatures, while ρu is reduced. The temperature dissipates quite rapidly in the direction perpendicular to the flap surface.

It was pointed out earlier that the thermal control is slightly less effecive at the side of body, particularly in the case of PR=6.4 and TR=4. Inspection of Figure 3.3a suggests that the tip vortex at the IB edge of the flap is quite sizeable at the highest temperature. Varying input temperature along the span is examined next in order to fix this local deficiency. Relative to the TR=4 case, the temperature level is lowered to TR=2 inboard over a nozzle segment corresponding to 1/16 of its span length. The results of this simulation are shown in Figure 3.4. The temperature footprint on the flap clearly marks the segemnt of the nozzle along which the temperature was lowered. The separation pattern inboard resembles that of the cold air supply in Figure 3.3a and the lift indicates slight improvement relative to the whole hot supply of TR=4. This test demonstrates that the hot air supply can be fine tuned to meet specific design requirements.

3.2 Combined Hot/Cold Supply

A variant of the thermal actuation, which aims at protecting the flap skin from excessive temperature levels, employs a mix of hot and cold air supply. The case of combined hot/cold supply having TR=4/1

and pressure of PR=6.4 is considered next. The hot air is provided through the inner segment of the inlet. The inlet area of the hot core flow is the same as the outer area of the cold supply. Therefore, this actuation results in an input mass flow of 75% of the equivalent whole cold supply ($0.5 \cdot 4^{-1/2} + 0.5 \cdot 1$). Figures 3.5 and 3.6 show the results of this hot/cold supply pattern. Compared to the whole hot supply, the partial hot supply where the hot jet is shrouded by a stream of cold air helps reduce the temperature levels on the nozzle walls and the flap surface. The reduction in mass flow is not as big as the whole hot TR=4 case. Nevertheless, the momentum coefficient of the hot/cold supply is consistent with the other modes of the thermally controlled actuation (Figure 3.6b).

4. Traverse Actuation

This section focuses on more efficient control based on the traverse actuation described in Reference 2. The analysis starts off by considering discrete stationary jets, followed by a set of traverse actuation modes.

4.1 Stationary Jets

A systematic approach is used to guide the implementation of the traverse actuation method in a general three-dimensional setting using the computational grid with the CD nozzle on the IB flap. The effect of discrete stationary jets is first considered. The jet sizes correspond to 1/8 the length of the nozzle (designated p1/8). The jets are placed at the IB and OB edges of the CD nozzle as well as in its middle segment. In addition, the results of the simultaneous application of the three jets is also presented. The results obtained with PR=4.8 are shown in Figure 4.1. Generally, the jets are effective in locally attaching the flow up to the trailing edge of the flap. The separate jet applications result in small increments in lift. Note that the IB and middle jet applications result in similar lift gains. The jet at the OB nozzle section helps in improving the flow on the OB flap, most likely due to the stronger spanwise effect on the wing segment, which has higher trailing edge sweep. Nevertheless, even the lift gain due to the OB jet is fairly modest and close to the lift produced by the whole nozzle actuation at the same mass flow. The lift gain by the combined jets is well below that of the whole nozzle actuation.

4.2 Single Jet Traverse Actuation

The traverse actuation consists of a jet size of p1/8, which traverses the span of the CD nozzle, from one edge to the other. In a sense, it can be viewed as a continual actuation amongst the states represented by the stationary jets from Figure 4.1. The jet frequency is $10H_z$ and it traverses from outboard to inboard. Figure 4.2 shows the instanteneous flow field during the limit cycle and the lift compared to the discrete jet actuation modes. The crossflow motion produces momentary flow attachment in the region around the respective wing section. A lingering effect occurs, where the flow remains attached over a sizeable wing segment, extending to the trailing edge. The instantaneous pockets of attached flow exhibit a slanted pattern, consistent with the jet traveling inboard. The continuous actuation results in improved streamlining of the flow at the flap in a time-average sense. It also creates an induced ripple effect that helps attach the flow over the outboard wing segment. The combined effects increase global circulation, which results in greater lift production. The cases marked A, B and C in the lift plot represent the progression from a whole nozzle actuation, to a stationary small jet, and up to the traverse small jet, respectively.

4.3 Split Jet Traverse Actuation

The instantaneous flow field in Figure 4.2 obtained with the single jet actuation shows significant flow variations along the span. These flow excitations have important implications with respect to structural integrity and fatigue. To produce a more uniform load distribution, an actuation mode obtained by splitting of the travelling wave into smaller elements is considered next. In this example, the traversing jet

p1/8 is split into 4 wavelets and it operates at the same frequency. Since it uses the same jet velocity, its mass flow rate is similar to p1/8. This pattern is denoted p1/8-w4. The results are shown in Figure 4.3. Although the flow is more uniform, there are remnants of flow separation close to the flap trailing edge. The results in Figure 4.4 demonstrate that higher effectiveness is achieved with the wider jets of p1/4-w4, resulting in a larger region of attached flow on the flap, but with larger actuation input.

The impact of the actuation pattern on the wing loading is analyzed in Figure 4.5. It presents the pressure distributions at two wing sections that cut through the flap elements. Specifically, these are the collective C_p over the actuation period, providing information on the oscillations experienced at the respective sections. It is noted that in a time-averaged sense the wing pressure is altered by the actuation due to global circulation. This is commensurate with the pressure contours in Figure 4.4 when compared to the baseline case. However, the oscillatory component of C_p strongly depends on the actuation pattern. In all cases, the perturbation diminishes quickly upstream, with almost no discernible oscillations at the leading edges. The largest amplitudes are confined to the IB flap element, and they are particularly large in the single jet case p1/8-w4. In this actuation, the OB flap experiences moderate pressure excitations. Split jet actuation patterns reduce the oscillation with nearly steady pressure on the IB flap.

4.4 Frequency Effects

The effect of frequency of actuation is presented in Figure 4.6. It shows the instantaneous flow structure obtained with the p1/4-w4 pattern at PR=4.8. The computed flow fields of the unactuated and the stationary blowing are also shown for reference. The stationary jets are only partially effective since they only affect the flow in their vicinity. The results of the traverse actuation underscore the impact of the frequency on the flow. In the case of traverse actuation, the lateral motion aims at killing off the separation in front of each jet packet. However, the flow reverts to its original separated state behind the jet packet. The traverse actuation exploits the flow latency during the reversion to the original flow separation state. At the appropriate actuation frequency (i.e., jet lateral speed), each jet element is able to cut into the separation bubble in the front at a greater rate than the regeneration of the separation pocket in the back. Moreover, the reversion to the original separation state is delayed by the following jet packet. Not surprisingly, improved flow is obtained with the 10Hz actuation frequency, which is consistent with the convective time scale of the flow (for the full-scale configuration) and marked by the red dash line in Figure 4.6.

The actuation is less effective at frequencies that are higher or lower than the characteristics frequency of the flow. At higher frequencies the actuation is less effective with limited impact on the separation pattern. In these cases, the interaction between the oscillatory jet and the ambient flow is virtually invariant on the global time scale and therefore, the flow on the flap is effectively decoupled from the operating frequency. In other words, the jets move so fast that the surrounding flow doesn't have enough time to react to the excitation. Lower frequencies also result in relatively limited improvement, in which cases, the individual jet cuts into the separation bubble in the front at a slower rate than the regeneration of the separation in the back. In the limit of very low frequency, the flow resembles stationary waves.

4.5 Direction of Jet Travel

To assess the effect of direction of jet travel, it is instructive to inspect the flow fields obtained with stationary waves for both the single jet and the split jet patterns. The flow fields for p1/8-w1 and p1/8-w4 are shown in Figure 4.7 in the perspective, rear and top views. Both actuation modes produce a slanted pattern of elongated attached flow regions emanating from the jets and extending to the trailing edge. The split wave actuation produces a checkered pattern of attached and separated flow pockets.

The effects due to the direction of jet travel are presented in Figure 4.8. Generally, the inboard travel is more effective than outboard, particularly in the lower frequency range. Referring to the stationary wave pattern, the inboard actuation is advantageous since it cuts through the larger separation in front of the jet packet. The difference is less pronounced at higher frequencies, where the actuation is decoupled

from the global flow. Nevertheless, operating close to the characteristics frequency is most effective, regardless of direction of travel.

4.6 Thermal Traverse Actuation

Since the thermally controlled actuation can be applied to any fluidic based actuation, the effect of high temperature supply is analyzed next in conjunction with the traverse method. Figure 4.9 shows instantaneous flow fields obtained for several traverse actuation modes with PR=6.4 and for TR=1 and 2. Here the whole nozzle blowing case described in Section 3.1 is also presented for reference. The pressure distributions and the separated flow patterns show very similar flow structure between the cold and the hot supply cases. The flap surface experiences momentary hot spots in the wake of the moving jets as they periodically impinge on the surface. The corresponding lift forces are shown in Figure 4.10. The reduction in mass flow obtained with the thermal/traverse actuation is very similar to that obtained for the long CD nozzle (Section 3.1, Figure 3.1). Specifically, the dashed pink line in Figure 4.10a connects the cold and hot supply cases of Figure 4.9 obtained with PR=6.4.

5. Comparison Between the High-Lift and the Vertical Tail

At this point, it is instructive to assess the validity of the predictions developed in this contract. This is facilitated using the study of Reference 9 in which the computational tool has been validated with measured data obtained for the AFC application to the vertical tail of the airplane. That application used a system of FOs to control flow separation on the vertical fin when the rudder is deflected, essentially similar to the simple hinge flap application in this study. The computational predictions of side-force due to AFC and the mass flow to achieve it were well correlated with the measured data. This pertains to measured data on a full-scale model obtained in a test conducted at the NASA NFAC wind tunnel, as well as the flight test of the Boeing 757 ecoDemonstrator (ecoD). In both cases, the mass flow required for actuation was about 3.2 lb/s for the respective side-force increments when the rudder was deflected at 30°. According to the current high-lift study the predicted mass flow for the 30° flap deflection using a system of FOs is approximately 36 lb/s, which is beyond the available resources onboard and thereby impractical. This is shown in the lift plot in Figure 5.1 by the dashed black curve at C_L~1.66. This data was obtained in the previous phase of the contract and reported upon in Reference 3. Clearly, there is a major discrepancy in the actuation mass flow between the vertical tail and the high-lift applications.

For a consistent comparison, however, the values of the mass flow have to be properly scaled in order to account for major differences between the two setups. Figure 5.2 presents specifics of the scaling up of the vertical tail data by considering several factors: the differences in the actuated area of the tail and the wing, free stream velocities, supply temperature and the incremental lift gain (in percentage) due to AFC. Interestingly, the projected mass flow from NFAC and ecoD are 30.8 lb/s and 40.5 lb/s, respectively, and generally consistent with the CRM level. In fact, the mass flow values from the vertical tail applications straddle the predicted mass flow for the CRM. The upshot of the scaling process is that the computed estimates of AFC performance of the simplified high-lift system can be viewed as reasonable predictions of realistic conditions for the nominal landing condition.

An interesting point with regard to the vertical tail application is in order. Since the current study has led to AFC implementations with significantly reduced mass flow, it is conceivable that the actuation input for the vertical tail could likewise be reduced. For example, using a larger rudder deflection in combination with other variants of fluidic actuation.

6. Conclusions

The analysis in this phase of the contract focused on the nominal landing condition for simplified wing/fuselage configurations. The nominal configuration employs a flap system at 50°. AFC has been applied to the IB flap element. Although target lift is achievable with AFC, the challenge of attaining it with very low input is still outstanding. Major findings from the simulations performed to date are summarized here.

Baseline configuration

Since flow control is particularly effective in reducing flow separation, revised baseline configurations with sizeable separation in the uncontrolled mode have been evaluated.

- Larger flap deflection of 70° results in mass flow reduction of approximately 17% at the target lift level relative to the nominal baseline with the flap at 50°.
- A 25% longer flap results in mass flow reduction of approximately 14% relative to the nominal baseline.

Incorporating higher flap deflection and longer chord can potentially lead to a cumulative reduction of about 30% in mass flow.

Traverse actuation

Several parameters have been identified for most efficient actuation:

- Inboard travel of the jets is more effective than travel in the outboard direction.
- Split waves result in more even distribution of perturbations along the span. This is advantageous since the milder flow excitations have important implications to wing structural integrity and fatigue.
- Highest performance is achieved when the actuation frequency is comparable to the convective time scale.

Thermal control

Higher air supply temperature results in reduced mass flow, proportional to $TR^{-1/2}$. Proper hot/cold inlet patterns offers advantages in shielding of the inner surfaces of the nozzle and the flap surfaces under the nozzle exhaust jet from high temperatures. This low-input method can be used with any fluidic device, including convergent/divergent ducts or fluidic oscillators.

Under normal operating conditions where an APU or engine bleed is considered for the AFC system, the air supply is at an elevated temperature relative to the ambient condition. It is therefore recommended to exploit the high temperature supply for reducing the mass flow required for actuation.

7. Next Steps

A set of recommendations are put forth in Figure 7.1, providing a pathway towards achieving the design target with practical input levels. The recommendations target a more adequate baseline configuration with new AFC layouts, primarily to utilize separation control while averting circulation control. Promising AFC concepts should be evaluated for a set of conditions representing high-lift operations and modelling of complete configurations. Finally, the design of actuation devices should be integrated into the wind tunnel model currently under development at NASA. Addressing these points is an essential risk reduction step towards a viable low input solution, increasing the odds for a successful demonstration of the AFC technology.

8. References

[1] Hartwich, P.M., Dickey, E.D., Sclafani, A.J., Camacho, P.P., Gonzales, A.B., Lawson, E.L., Mairs, R.Y., and Shmilovich, A., "AFC-Enabled Simplified High-Lift System Integration Study," NASA CR 2014-218521, September 2014.

[2] Shmilovich, A. and Yadlin, Y., "Traverse Actuation Method," AIAA Paper 2016-3309.

[3] Hartwich, P.M., Shmilovich, A., Lacy, D.S., Dickey, E.D., Sclafani, A.J., Sundaram, P., and Yadlin, Y., "Refined AFC-Enabled High-Lift System Integration Study," NASA CR-2016-219170, March 2016.

[4] Shmilovich, A., Yadlin, Y., Dickey, E. D., Hartwich, P. M., and Khodadoust, A., "Development of an Active Flow Control Technique for an Airplane High-Lift Configuration," AIAA Paper 2017-0322.

[5] Lacy, D.S., and Sclafani, A.J., "Development of the High Lift Common Research Model (HL-CRM): A Representative High Lift Configuration for Transonic Transports", AIAA Paper 2016-0308.

[6] Shmilovich, A., Yadlin, Y. and Clark, R.W., "Traversing Jet Actuator," US Patent 8,336,828, December, 2012.

[7] Shmilovich, A. and Kent, S. R., "Fluidic Traversing Actuator," US Patent 9,511,849, December, 2016.

[8] Shmilovich, A. and Whalen, E., "A Technique for Low Input Flow Control Actuation", to be presented at the 2017 AIAA Aviation Conference.

[9] Shmilovich, A., Yadlin, Y. and Whalen, E., "Numerical Simulations of an Airplane with an Active Flow Control System", AIAA Paper 2016-3929.

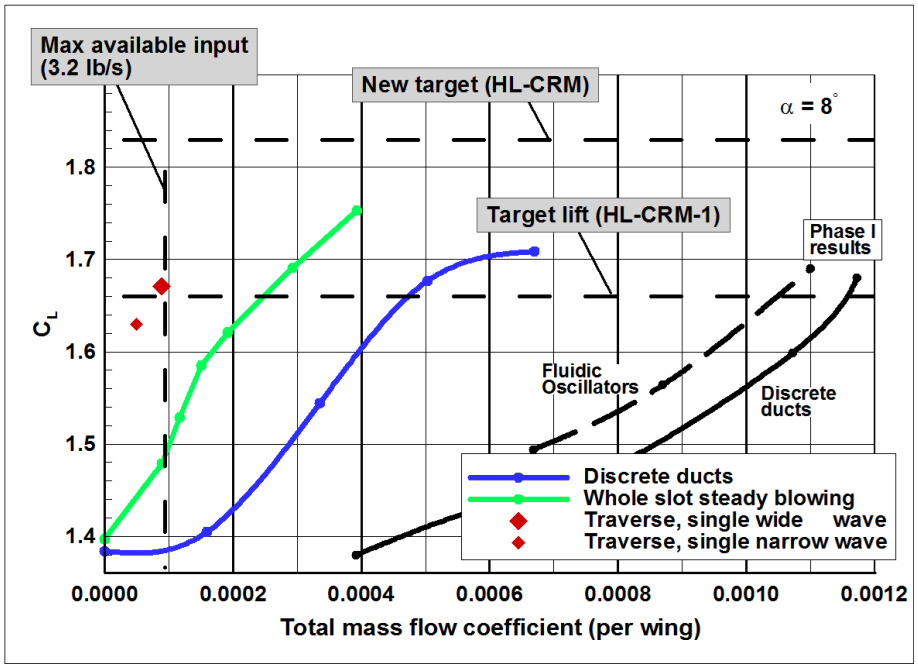

Figure 1.1. Summary of the findings from Phases I and II of the contract: lift of various actuation methods for the AFC-enabled simplified high-lift configuration.

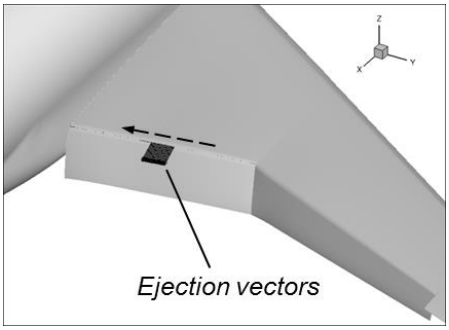

Figure 1.2. Traverse actuation (narrow wave).

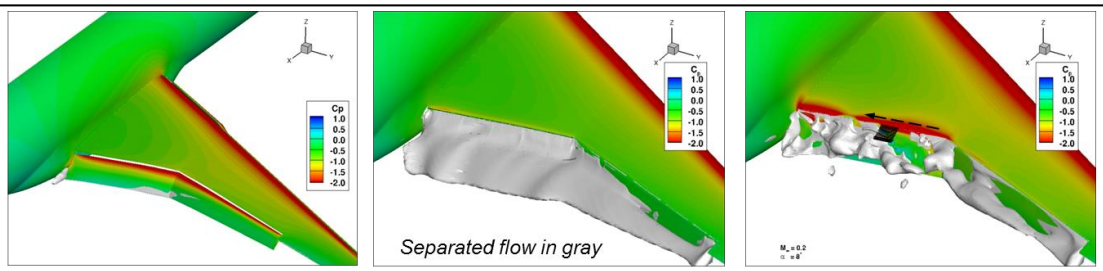

Figure 1.3. Flow fields at the nominal landing condition.

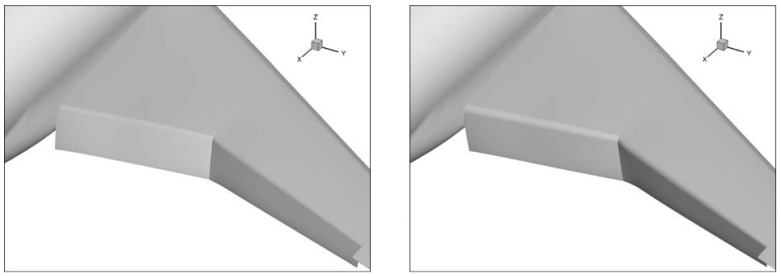

(a) δ_f = 50° (original) (b) δ_f = 70°

Figure 2.1. Baseline configurations with different flap deflections.

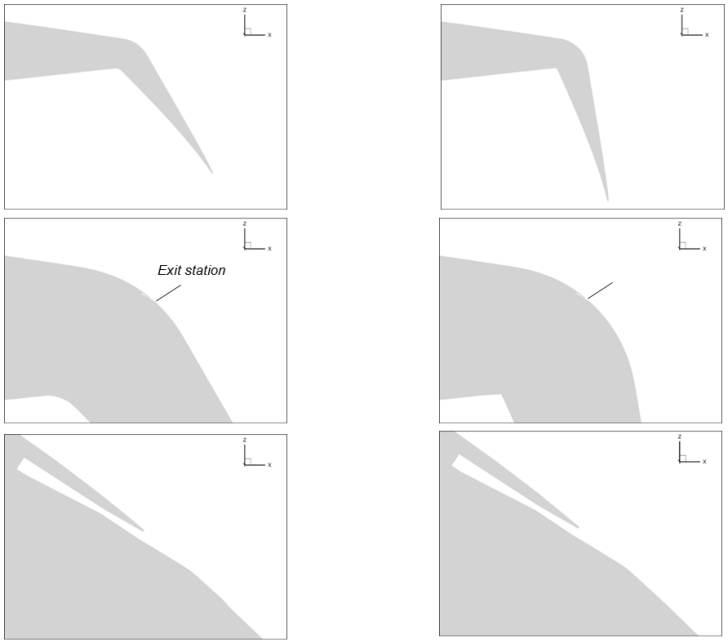

(a) δ_f = 50° (b) δ_f = 70°

Figure 2.2. Mid sections of IB flap with the nozzles at the nominal X1 location.

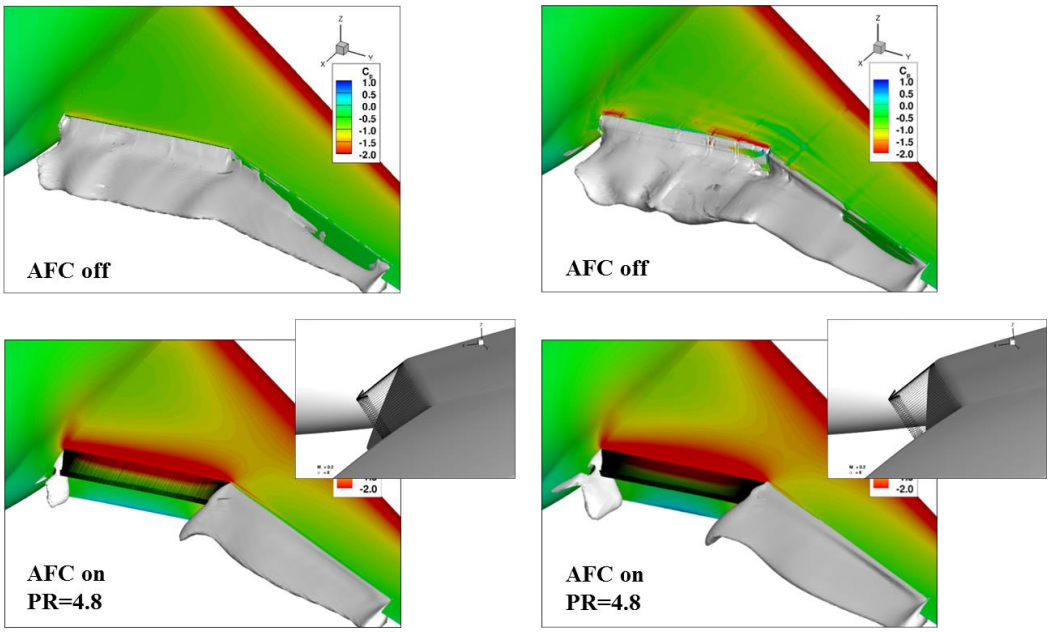

Figure 2.3. Flow fields obtained at different flap deflections.

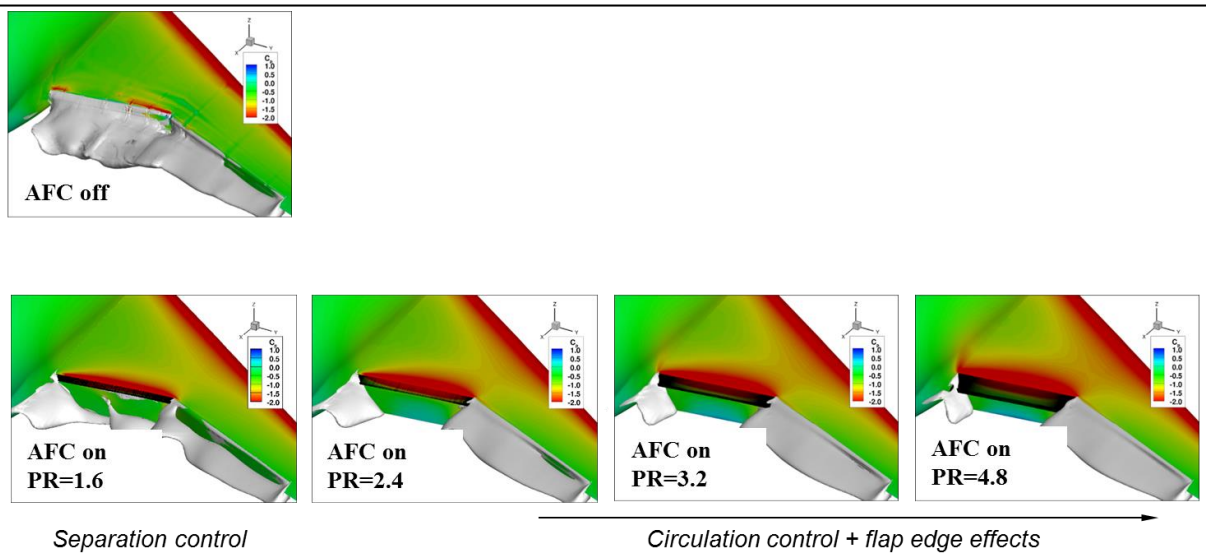

Figure 2.4. Flow fields for the 70° flap deflection at various actuation levels.

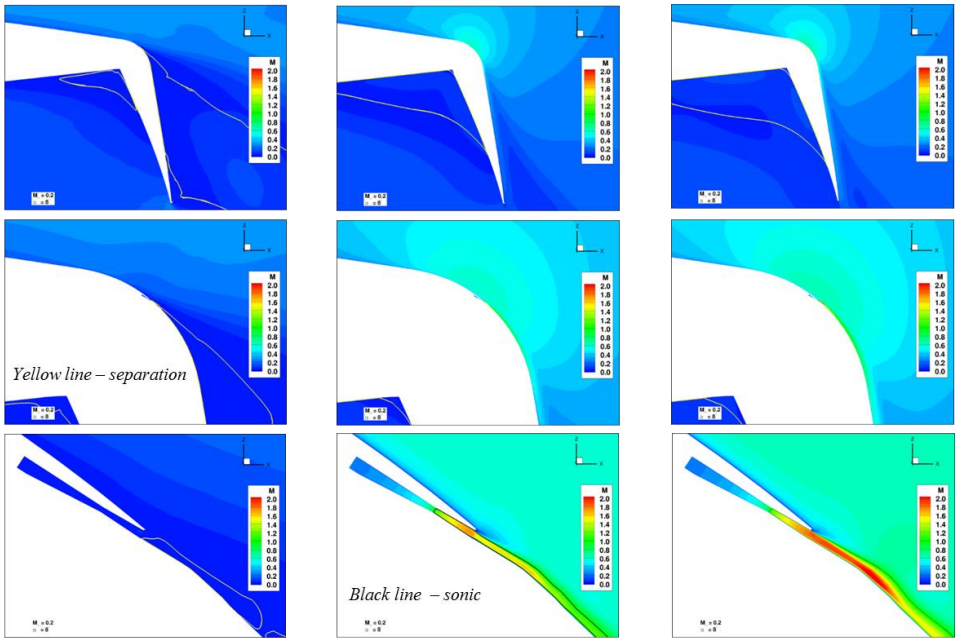

Figure 2.5. Flow fields in the mid sections of IB flap at the 70° deflection.

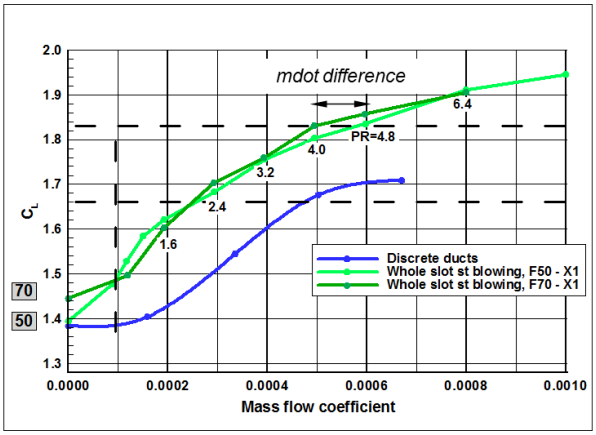

Figure 2.6. Lift gain due to AFC for the different flap deflections (CD nozzle).

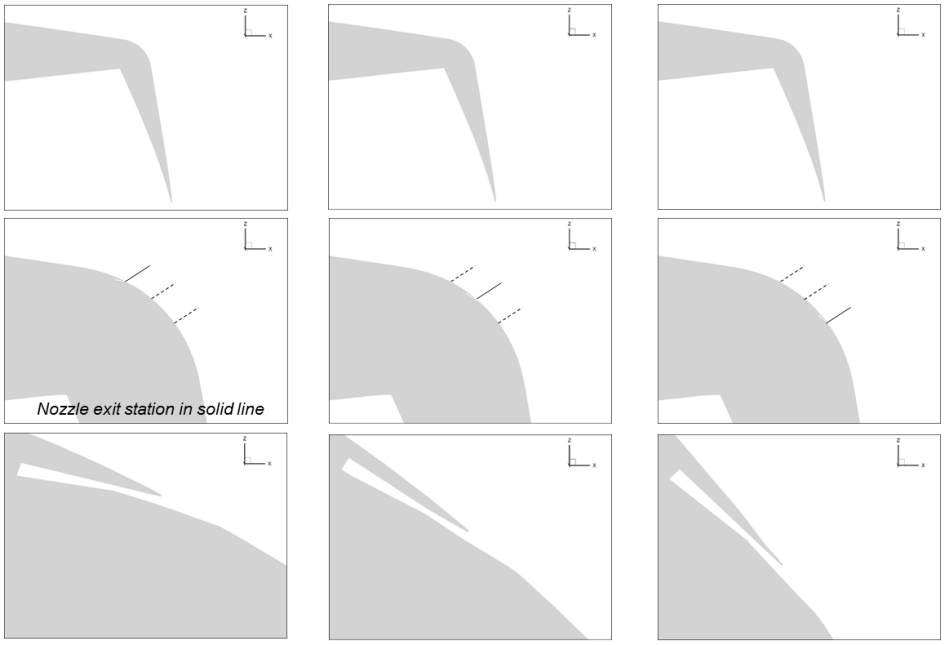

(a) X0
3.14" from X1 (0.84%C)

(b) X1 (nominal)
(85.8%)

(c) X2
3.35" from X1 (0.89%C)

Figure 2.7. Mid sections of IB flap with the nozzles at various locations (δ_f=70°).

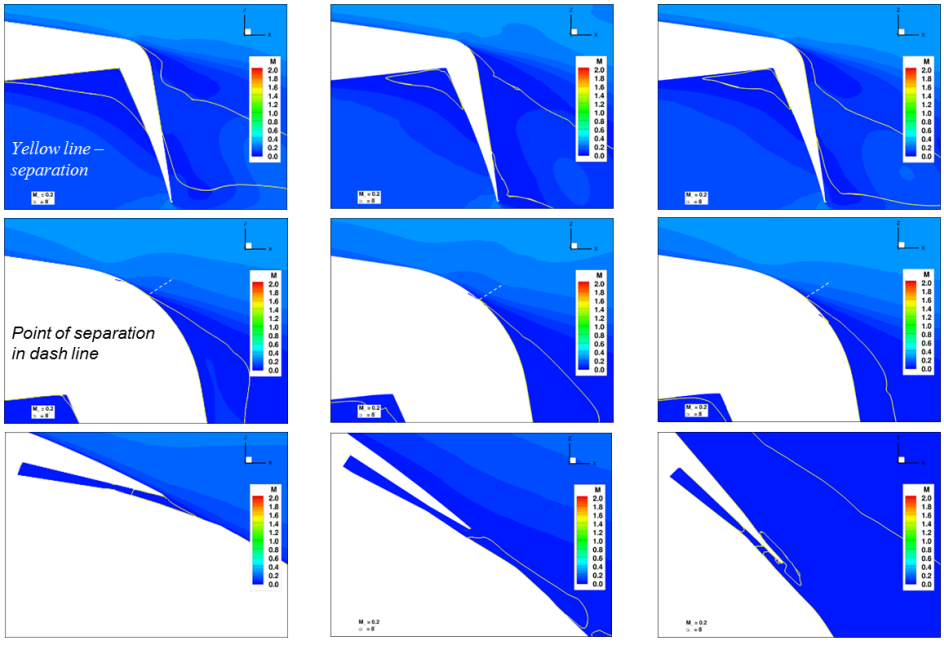

(a) X0

(b) X1 (nominal)

(c) X2

Figure 2.8. Sectional flow fields in the mid sections of IB flap with the nozzle at various locations – AFC-off.

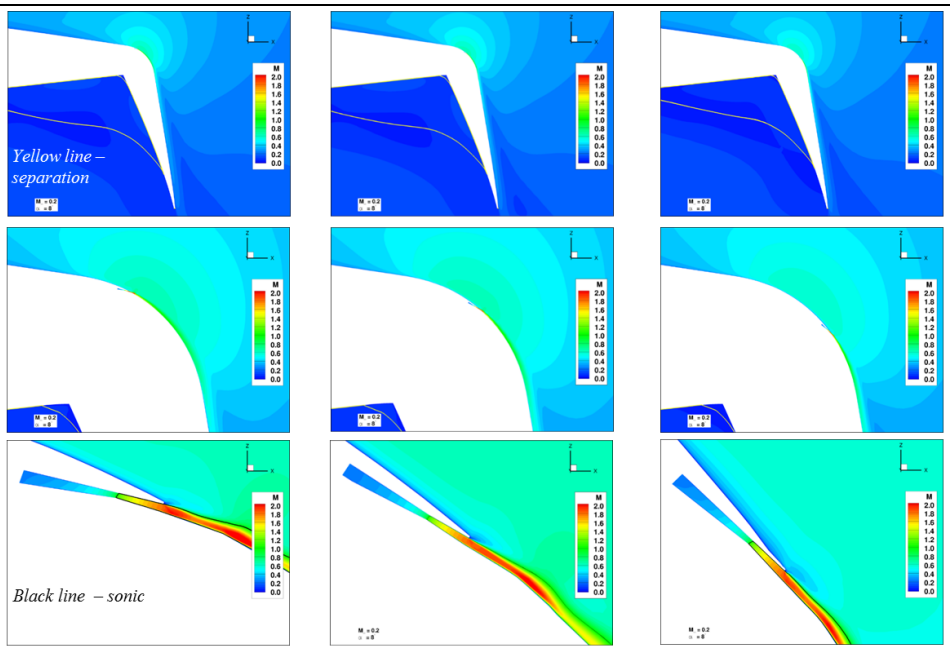

Figure 2.9. Sectional flow fields in the mid sections of IB flap with the nozzle at various locations – AFC-on, PR=4.8.

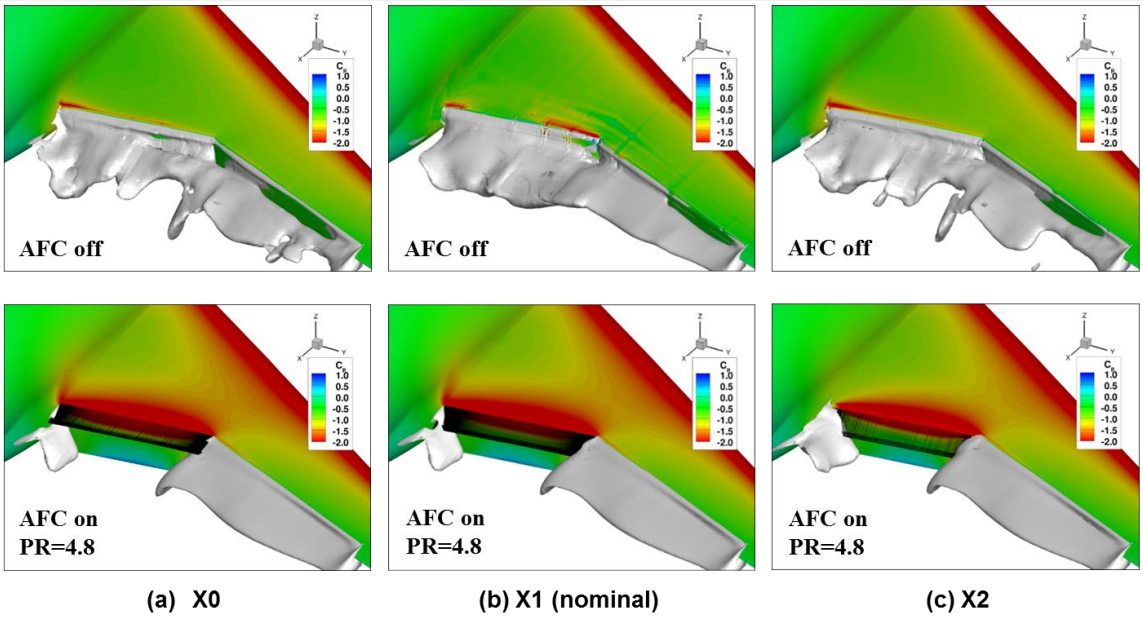

Figure 2.10. Flow fields for the various nozzle locations.

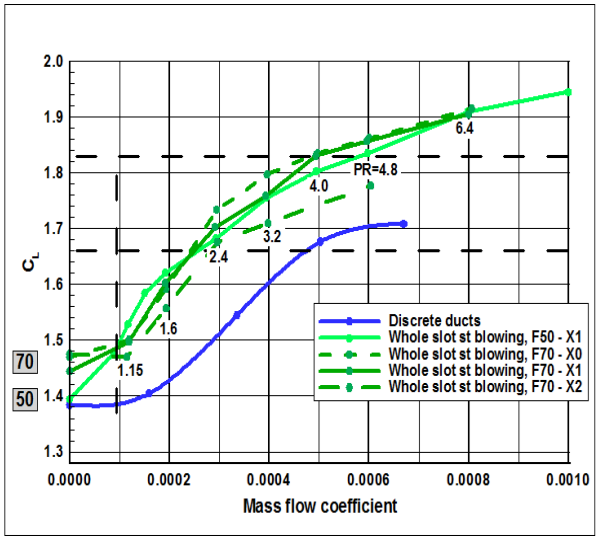

Figure 2.11. Lift gain for different nozzle locations for the 70° flap deflection (CD nozzle).

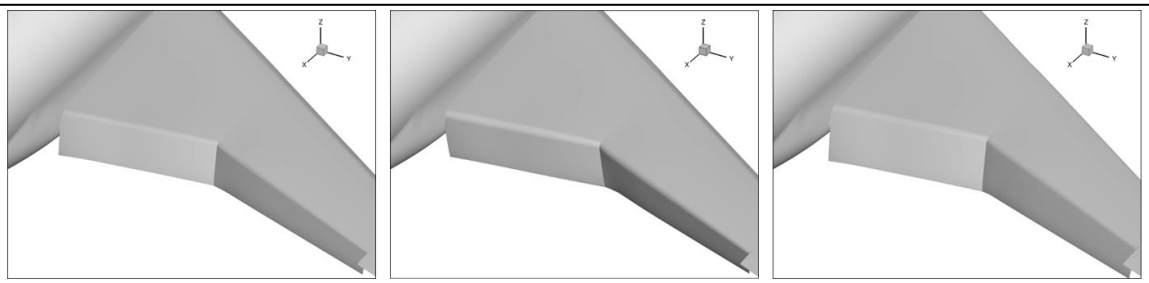

(a) δ_f = 50°, C_f = 1 (original)

(b) δ_f = 70°, C_f = 1

(c) δ_f = 50°, C_f = 1.25

Figure 2.12. Variants of the baseline configurations with different flap deflections and flap chord length.

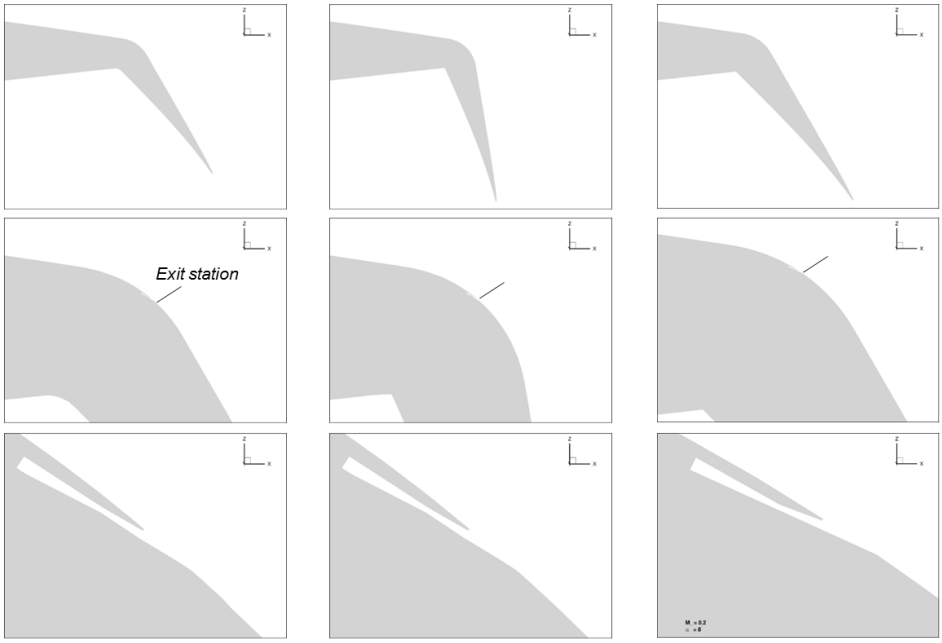

(a) δ_f = 50°, C_f = 1 (original) (b) δ_f = 70°, C_f = 1 (c) δ_f = 50°, C_f = 1.25

Figure 2.13. Nozzle layout for the various baseline configurations.

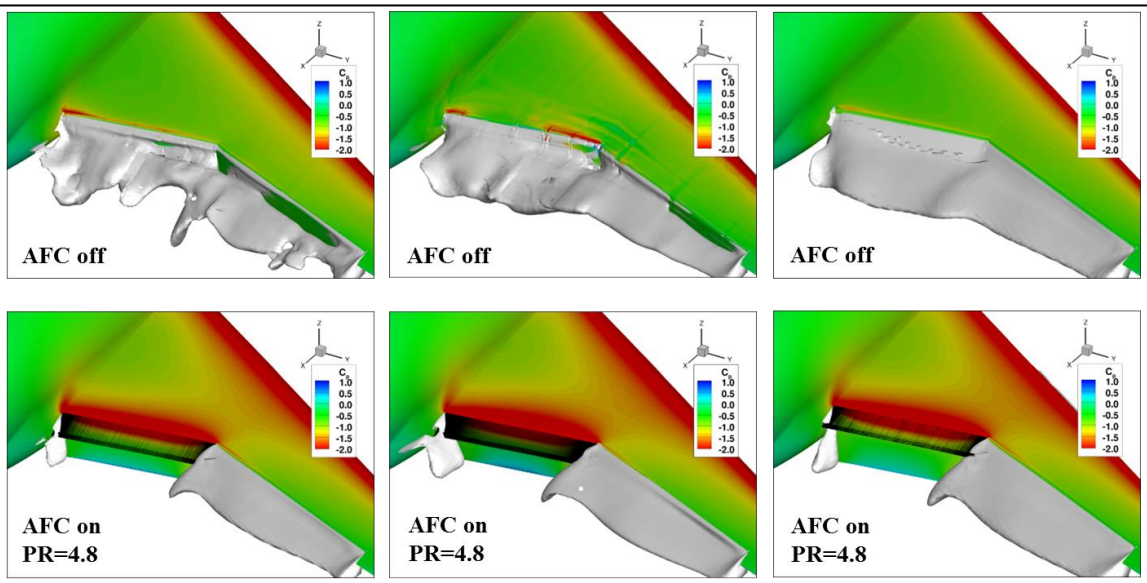

(a) δ_f = 50°, C_f = 1 (original) (b) δ_f = 70°, C_f = 1 (c) δ_f = 50°, C_f = 1.25

Figure 2.14. Flow fields for the various baseline configurations.

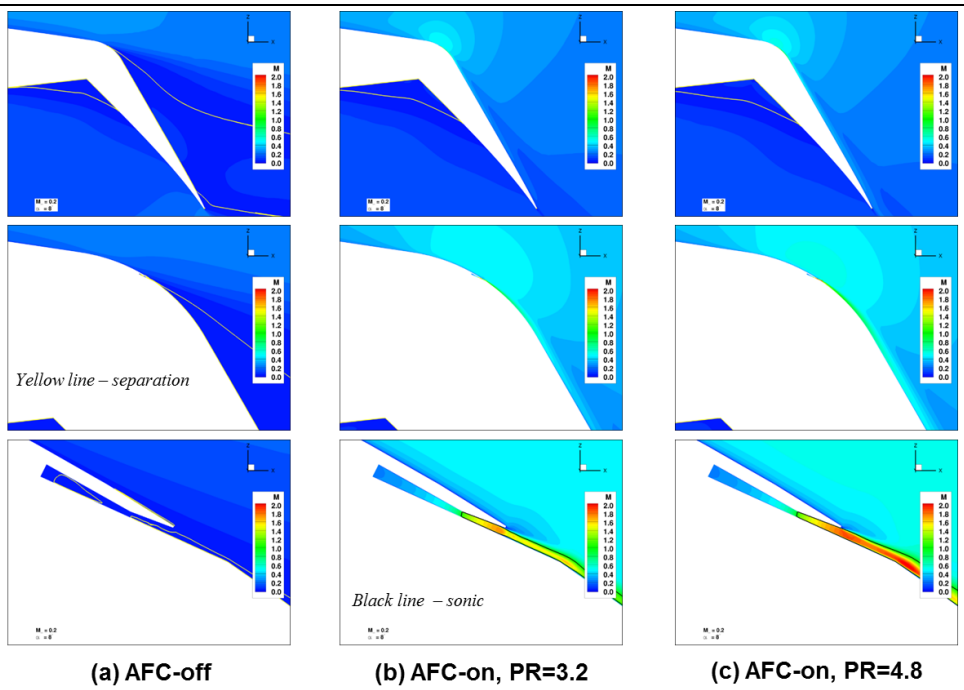

Figure 2.15. Flow fields in the mid sections of IB flap for the large flap configuration (δ_f = 50°, C_f = 1.25).

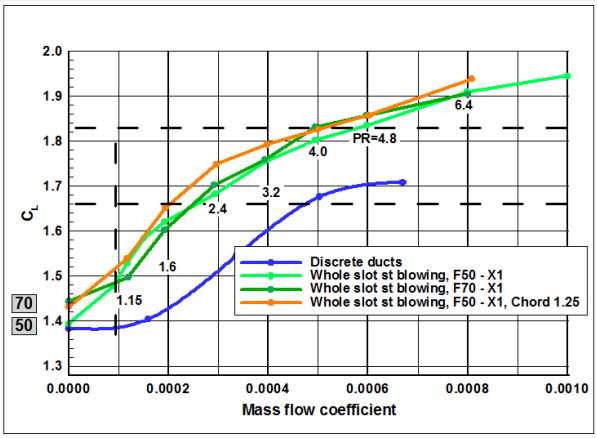

Figure 2.16. Lift gain for the different simplified configurations (CD nozzle).

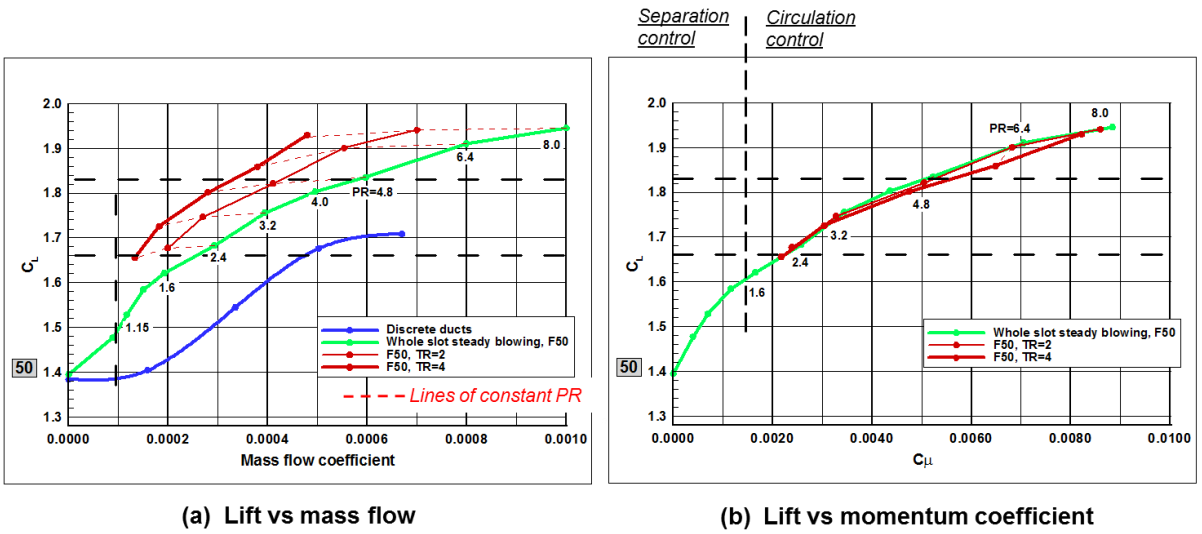

Figure 3.1. Effect of the thermally controlled actuation on lift.

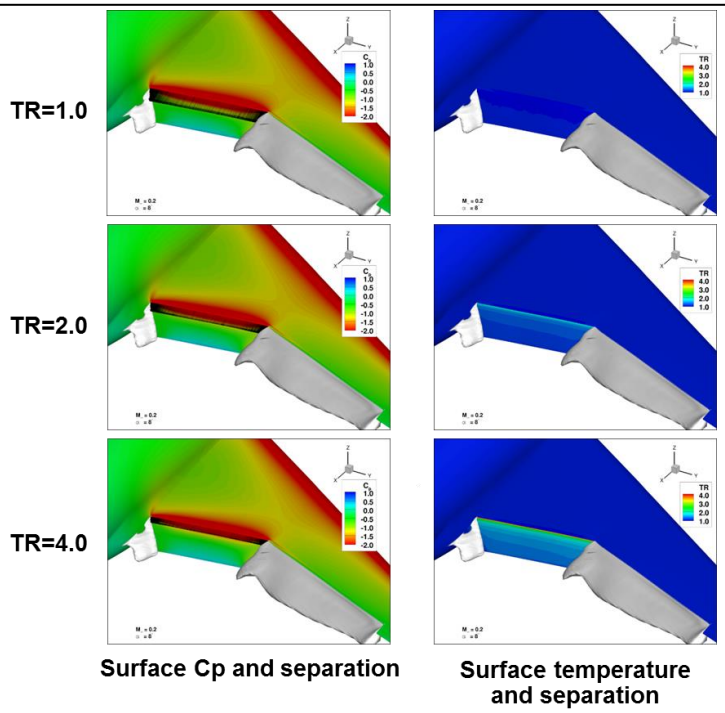

Figure 3.2a. Flow fields obtained with PR=3.2 and various supply temperature (cont.).

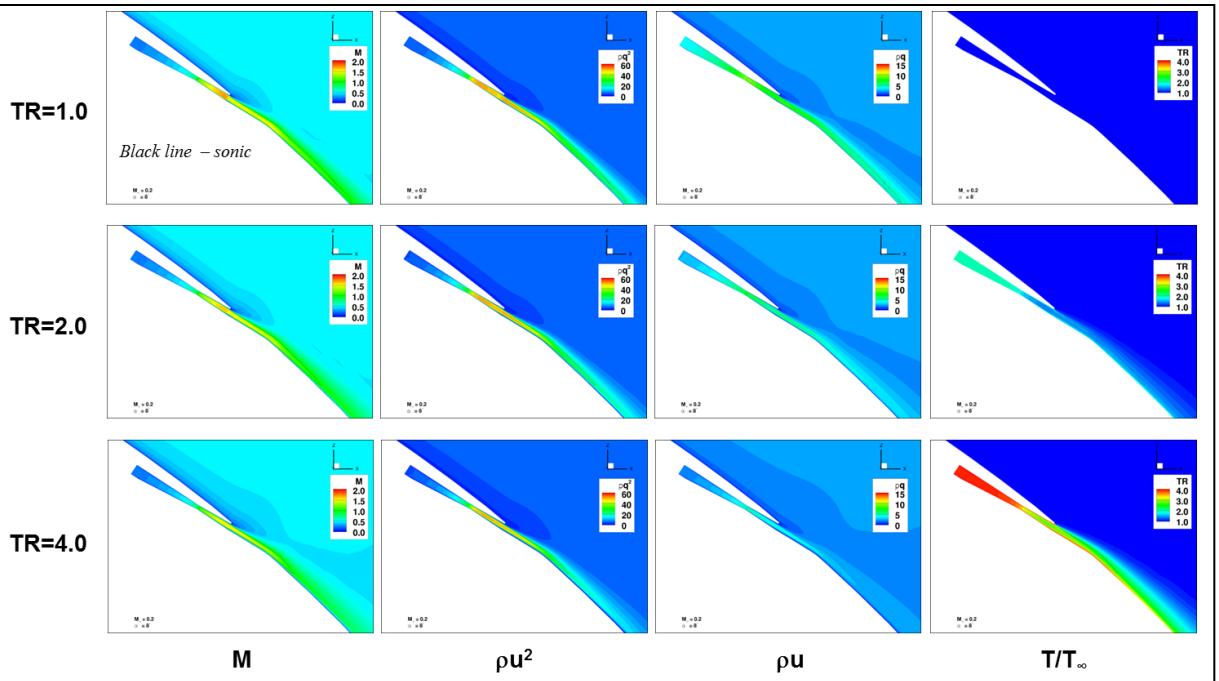

Figure 3.2b. Nozzle flow fields at the mid-section of the IB flap obtained with PR=3.2 and various supply temperature (concl.).

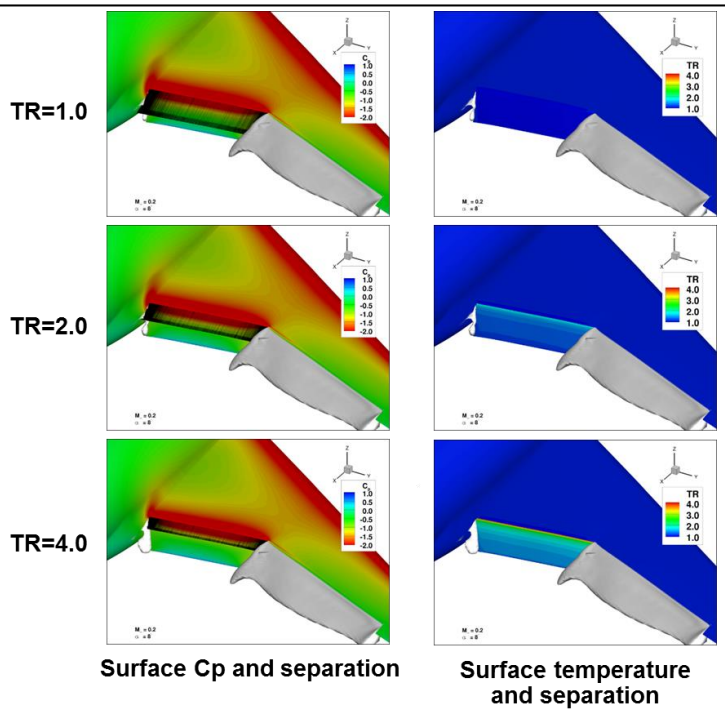

Figure 3.3a. Flow fields obtained with PR=6.4 and various supply temperature (cont.).

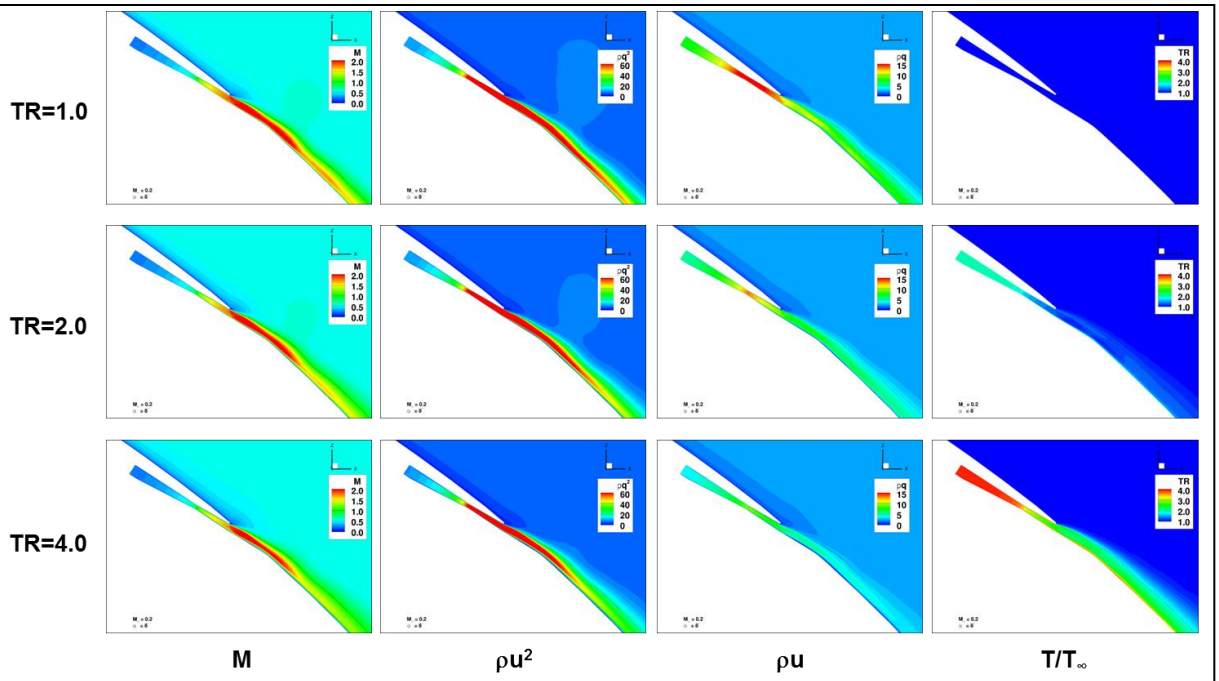

Figure 3.3b. Nozzle flow fields at the mid-section of the IB flap obtained with PR=6.4 and various supply temperature (concl.).

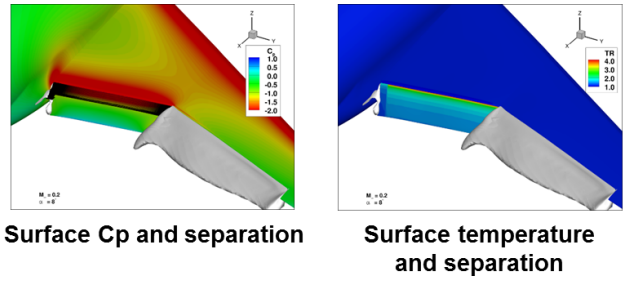

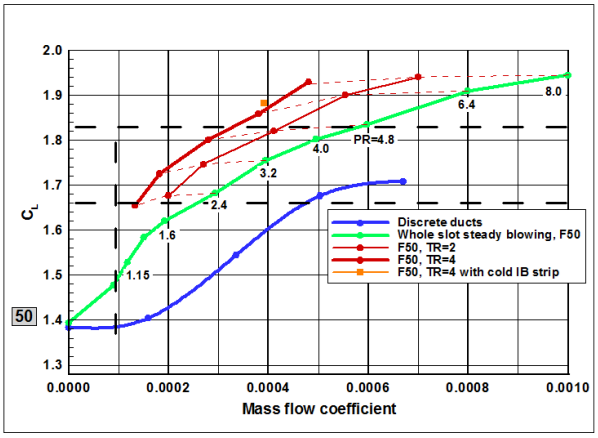

Figure 3.4. Hot supply of TR=4 with colder supply of TR=2 at the inboard strip of nozzle (PR=6.4).

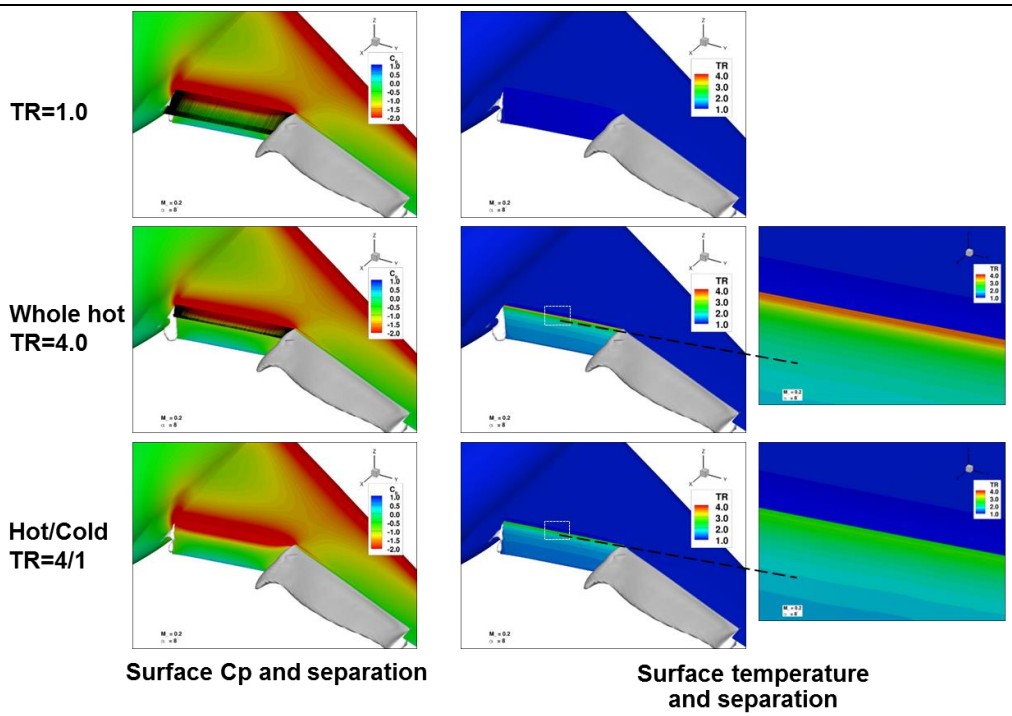

Figure 3.5a. Effect of hot/cold air supply. PR=6.4, TR=4/1 (cont.).

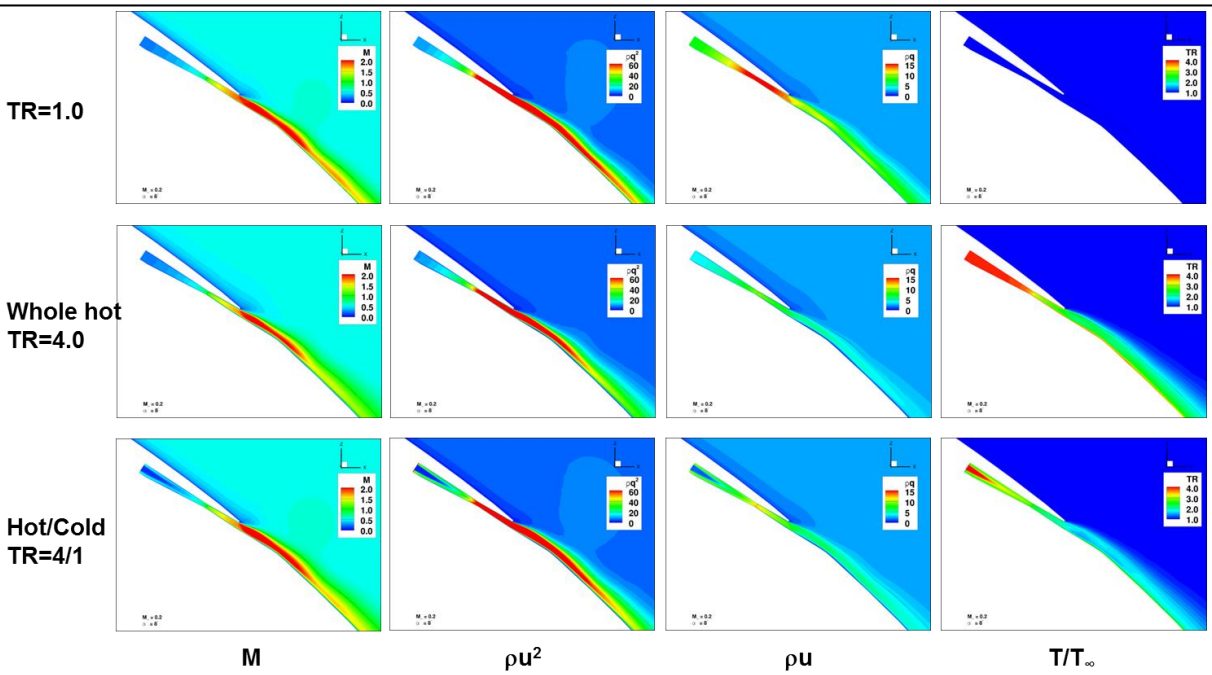

Figure 3.5b. Effect of hot/cold air supply on nozzle flow. PR=6.4, TR=4/1 (concl.).

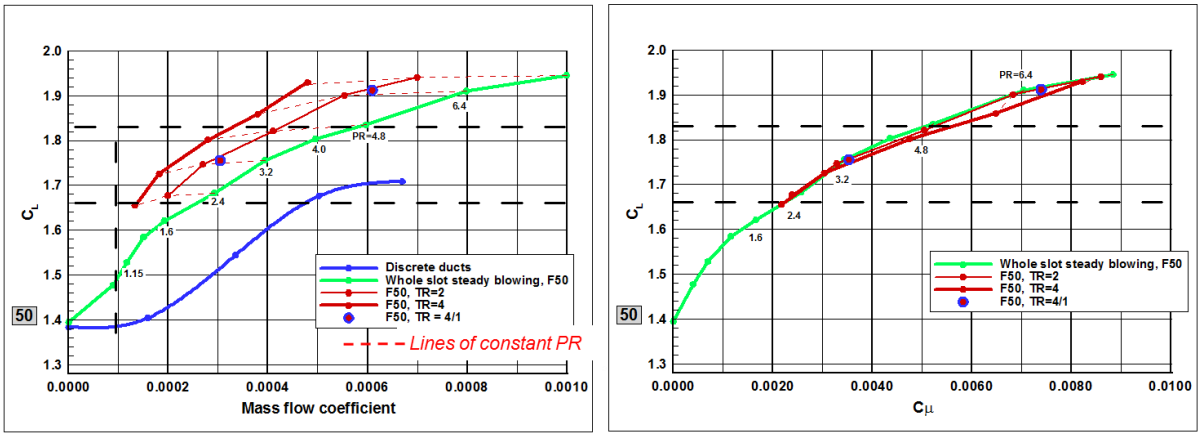

(a) Lift vs mass flow (b) Lift vs momentum coefficient

Figure 3.6. Effect of hot/cold air supply of TR=4/1 on lift.

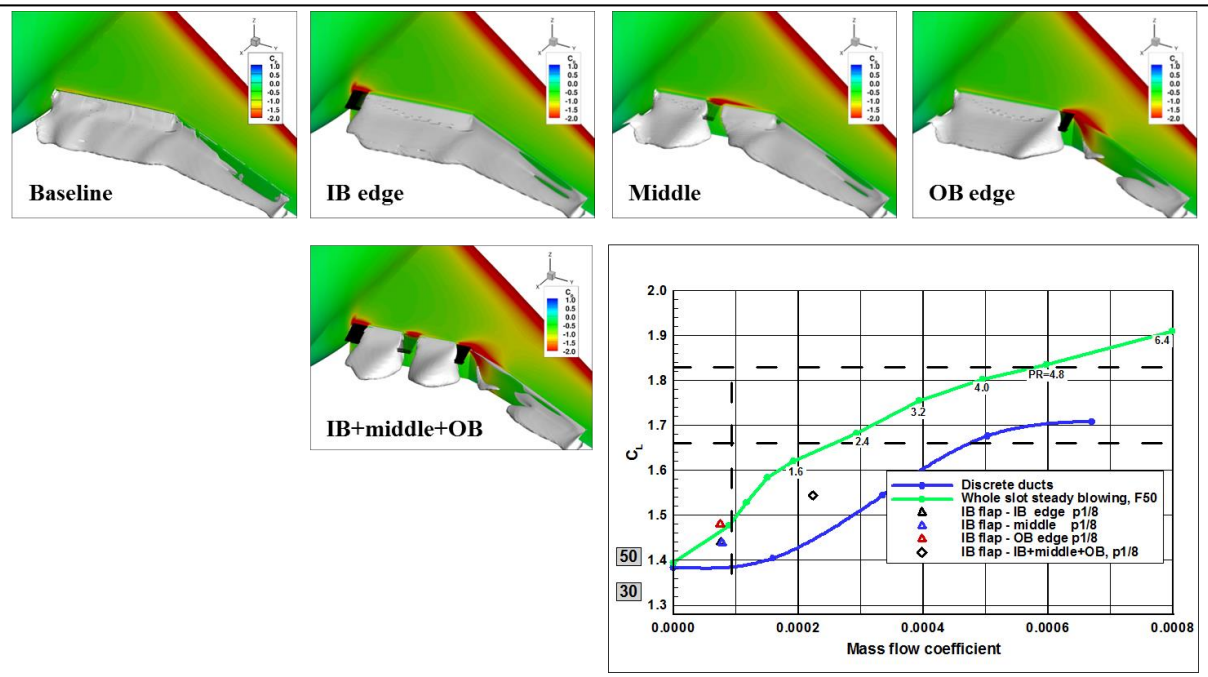

Figure 4.1. Effect of stationary jets placed at various locations along the nozzle (PR=4.8, p1/8).

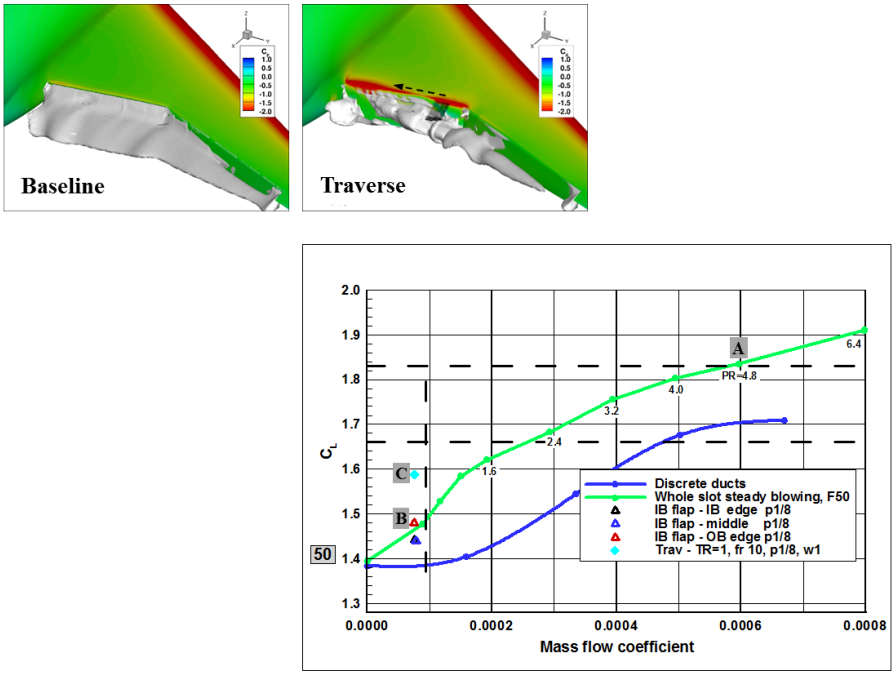

Figure 4.2. Effect of traverse actuation (PR=4.8, p1/8, 10Hz).

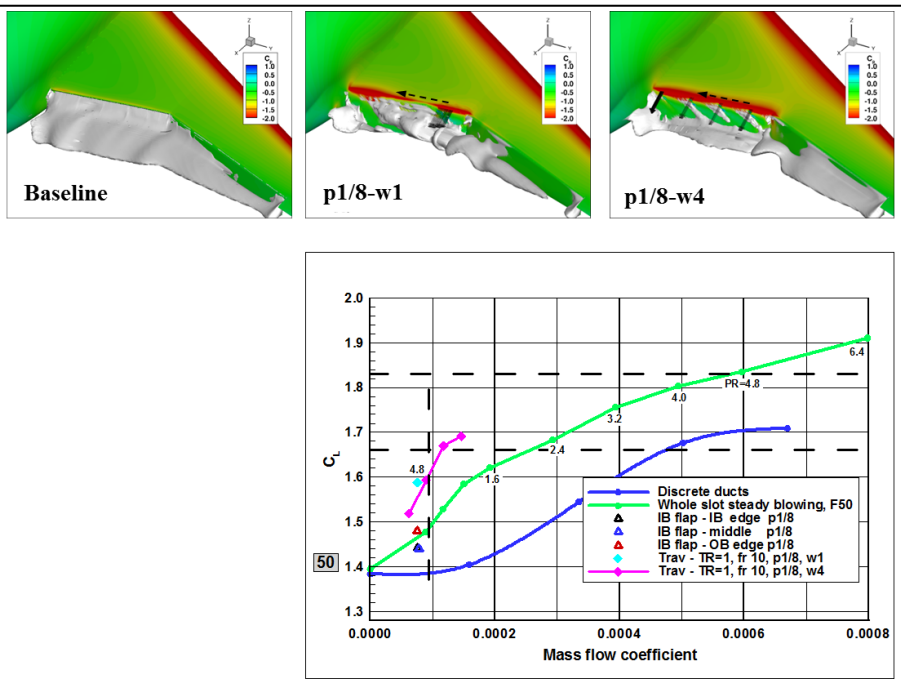

Figure 4.3. Effect of split wave actuation. Flow fields shown for PR=4.8.

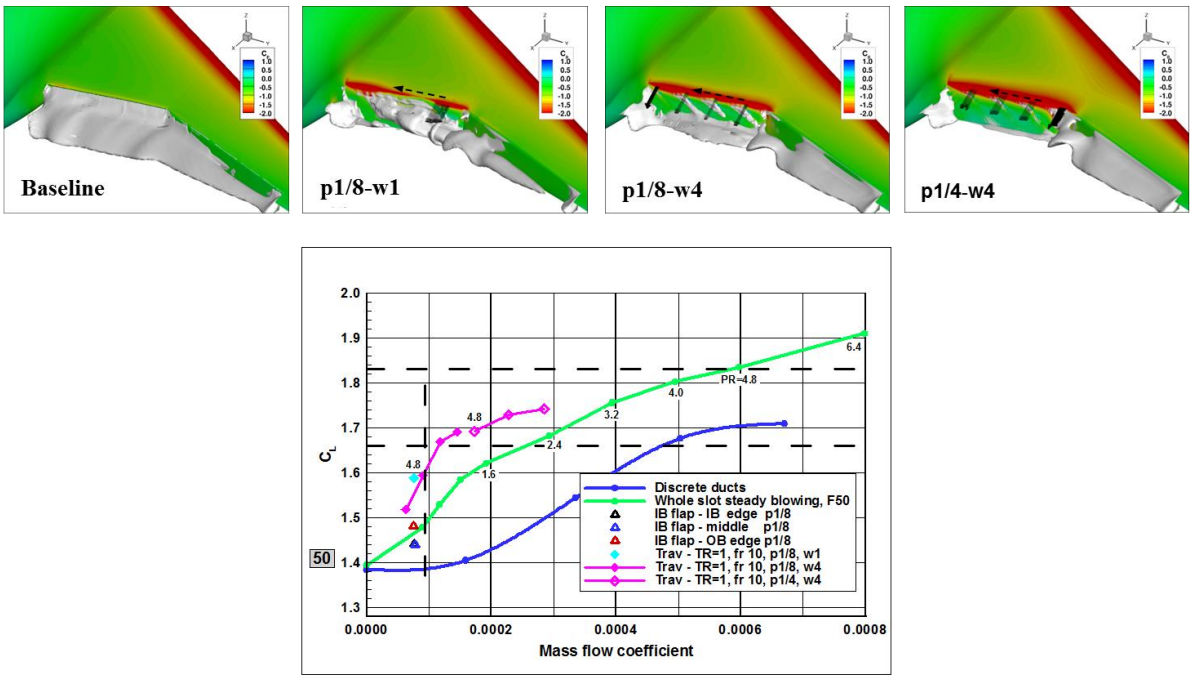

Figure 4.4. Effect actuation with wider split jets. Flow fields shown for PR=4.8.

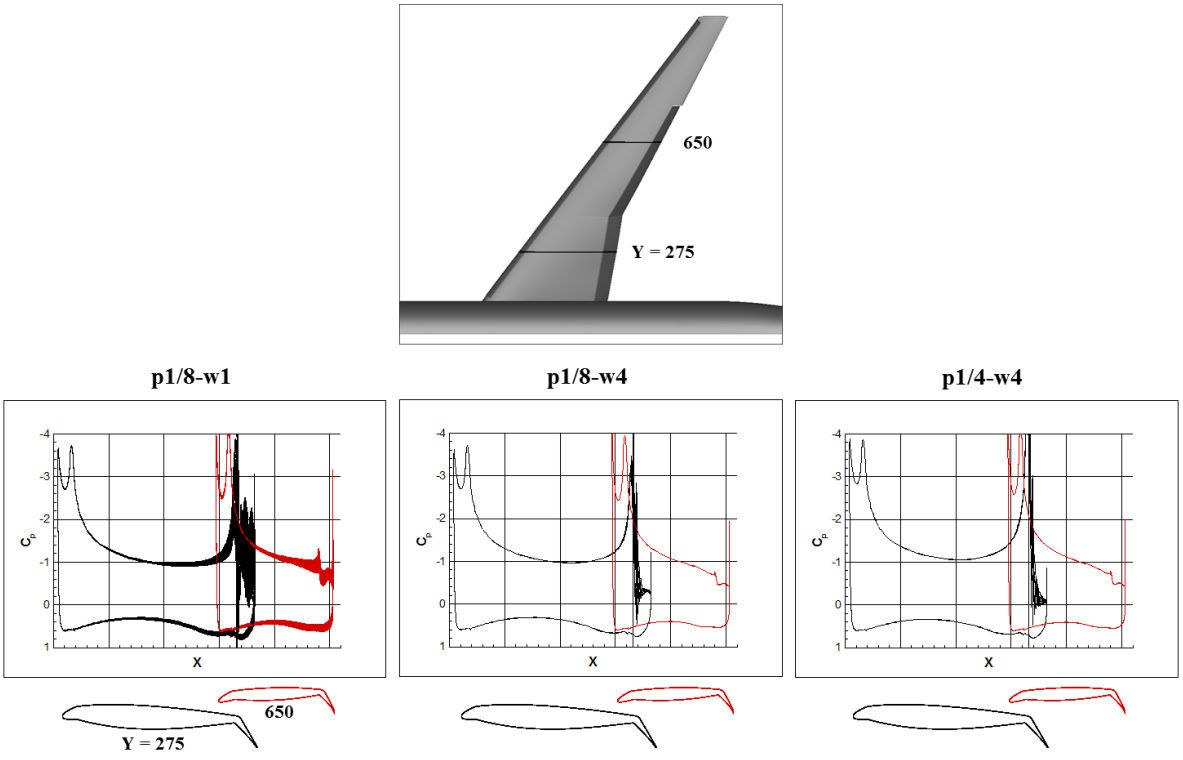

Figure 4.5. Limit-cycle sectional pressure distributions for the various traverse actuation patterns. PR=4.8.

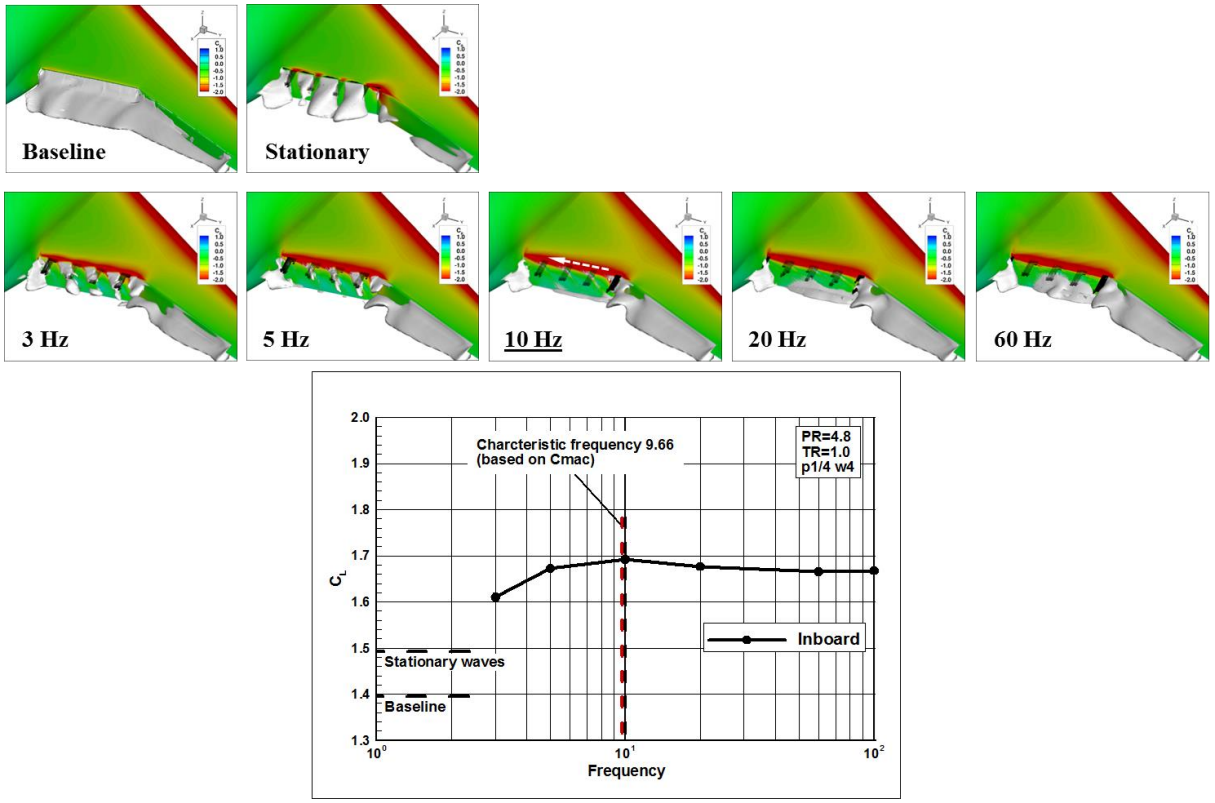

Figure 4.6. Effect of actuation frequency. p1/4-w4, PR=4.8.

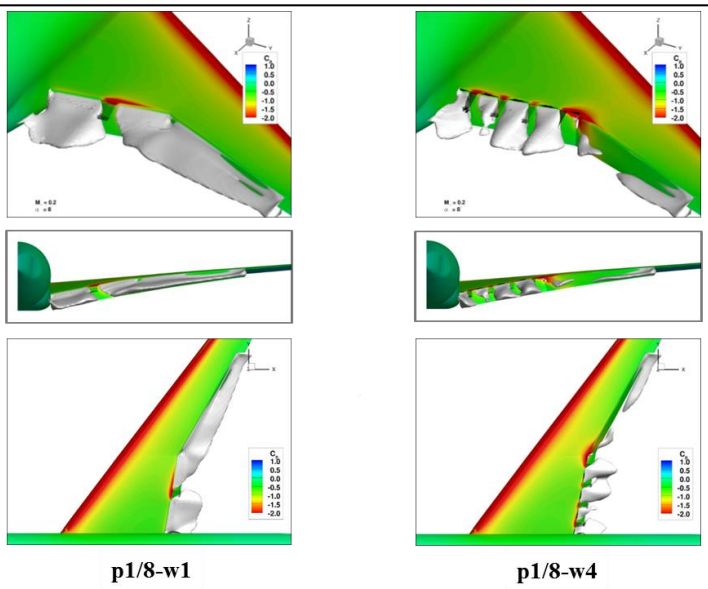

Figure 4.7. Flow fields due to stationary jets (PR=4.8).

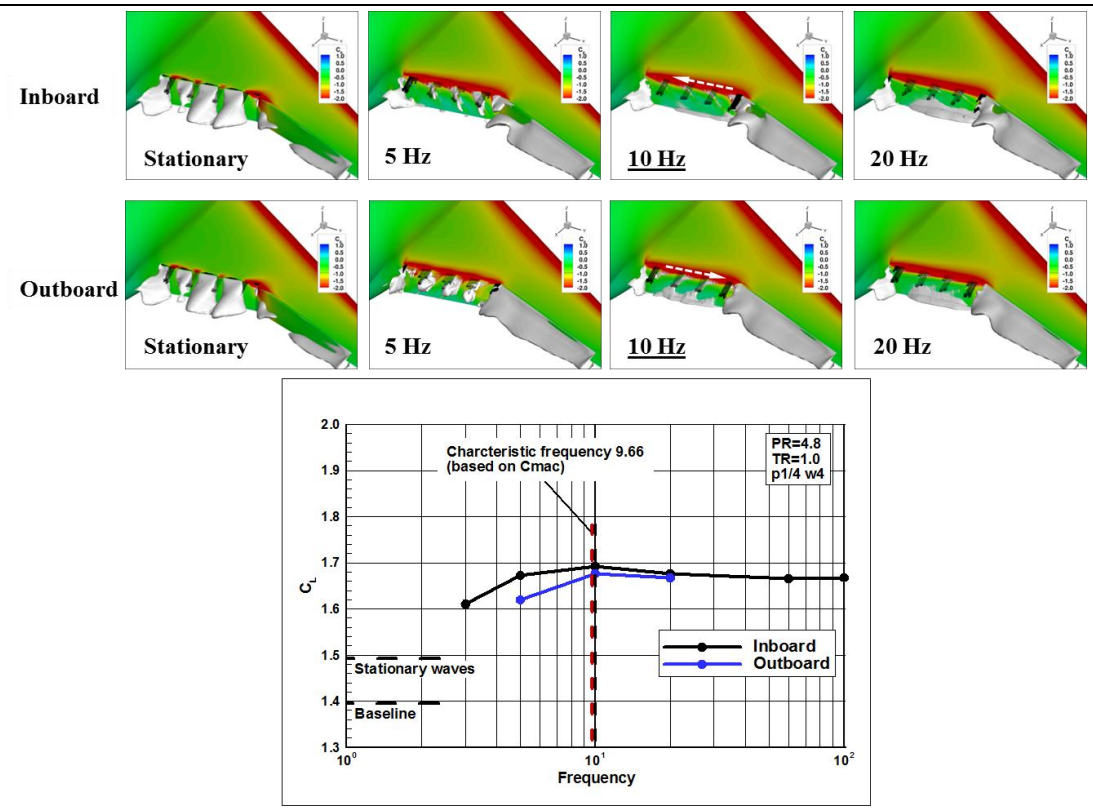

Figure 4.8. Sensitivity to the direction of travel (p1/8-w4, PR=4.8).

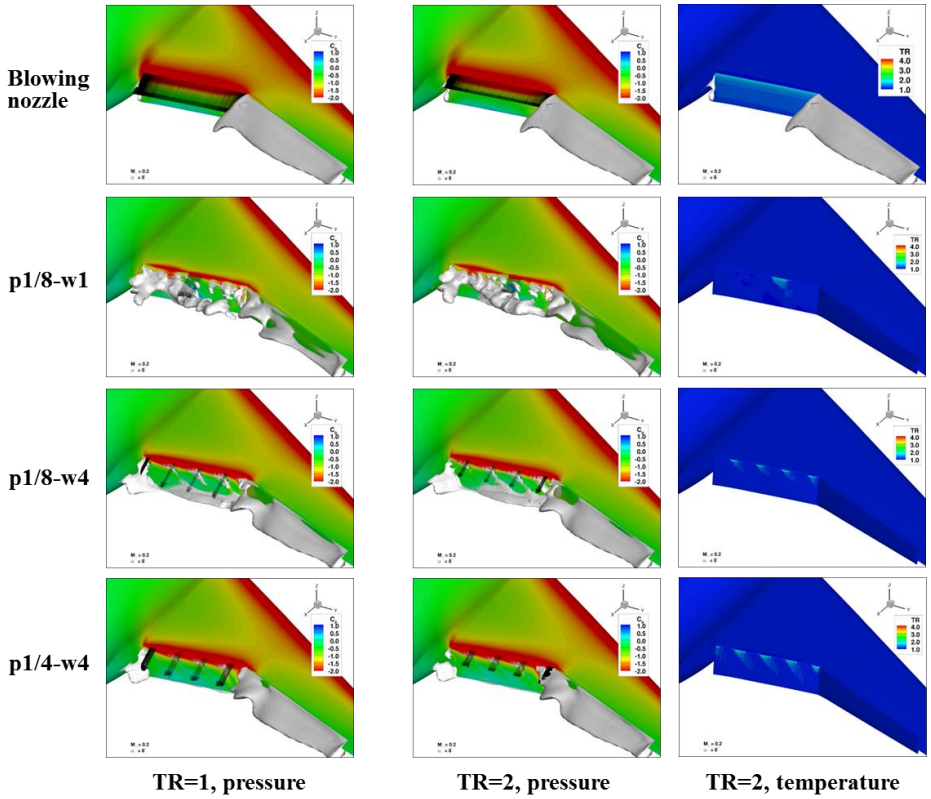

Figure 4.9. Combined traverse/thermal actuation, PR=6.4.

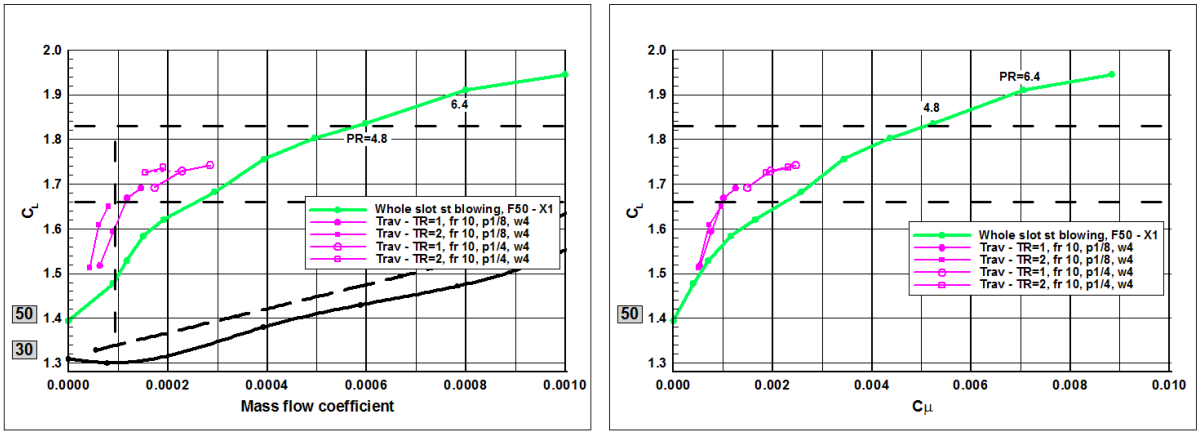

(a) Lift vs mass flow

(b) Lift vs momentum coefficient

Figure 4.10. Effect of combined traverse/thermal actuation on lift.

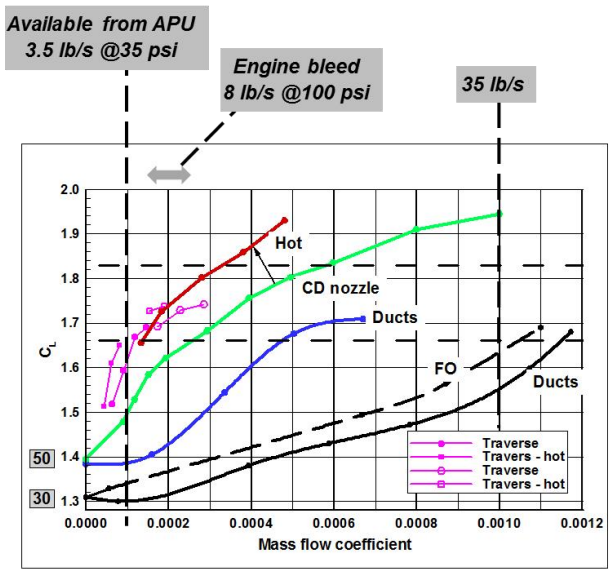

(a) CRM - Lift vs mass flow

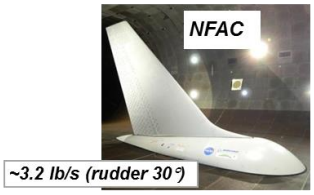

(b) Vertical tail – NFAC wind tunnel test

(c) Vertical tail – flight test (ecoDemonstrator)

Figure 5.1. Comparison in actuation mass flow for the current high-lift and the vertical tail data.

	NFAC	ecoD	AFC/CRM
Mass flow, lb/s	**3.2**	**3.2**	**36**
Area, in²	43,000	43,000	201,500
M_∞	0.151	0.176	0.2
TR	1	1.15	1
Objective $\Delta C_L/C_L$	20%	14%	31%*
Scaled up mass flow, lb/s	**30.8**	**40.5**	**36**

* Fuselage carries ~14% of total lift

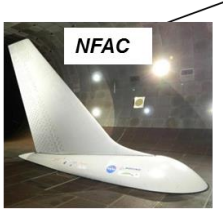

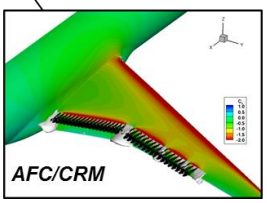

Figure 5.2. Proper scaling results in fairly consistent values of mass flow amongst the various AFC applications.

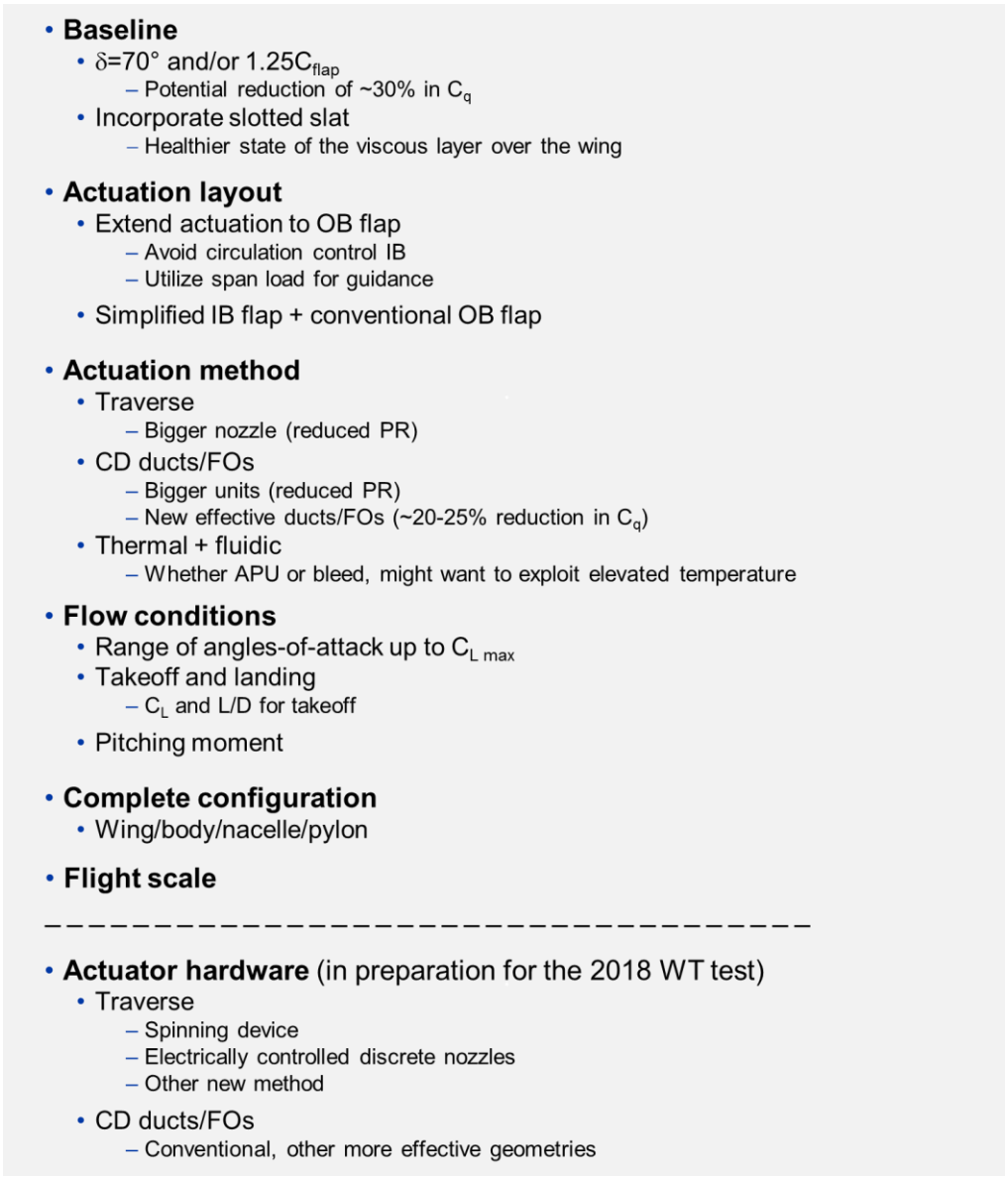

Figure 7.1. Next steps.

REPORT DOCUMENTATION PAGE

Form Approved
OMB No. 0704-0188

1. REPORT DATE *(DD-MM-YYYY)*	2. REPORT TYPE	3. DATES COVERED *(From - To)*
01- 07- 2017	Contractor Report	

4. TITLE AND SUBTITLE

Refined AFC-Enabled High-Lift System Integration Study

5a. CONTRACT NUMBER

NNL16AA04B

5b. GRANT NUMBER

5c. PROGRAM ELEMENT NUMBER

6. AUTHOR(S)

Shmilovich, Arvin; Yadlin, Yoram; Dickey, Eric D.; Gissen, Abraham N.; Whalen, Edward A.

5d. PROJECT NUMBER

5e. TASK NUMBER

NNL16AB02T

5f. WORK UNIT NUMBER

081876.02.07.02.01.04

7. PERFORMING ORGANIZATION NAME(S) AND ADDRESS(ES)

NASA Langley Research Center
Hampton, VA 23681-2199

8. PERFORMING ORGANIZATION REPORT NUMBER

9. SPONSORING/MONITORING AGENCY NAME(S) AND ADDRESS(ES)

National Aeronautics and Space Administration
Washington, DC 20546-0001

10. SPONSOR/MONITOR'S ACRONYM(S)

NASA

11. SPONSOR/MONITOR'S REPORT NUMBER(S)

NASA-CR-2017-219636

12. DISTRIBUTION/AVAILABILITY STATEMENT

Unclassified - Unlimited
Subject Category 34
Availability: NASA STI Program (757) 864-9658

13. SUPPLEMENTARY NOTES Langley Technical Monitor: John C. Lin

14. ABSTRACT

This project is a continuation of the NASA AFC-Enabled Simplified High-Lift System Integration Study contract (NNL10AA05B) performed by Boeing under the Fixed Wing Project. This task is motivated by the simplified high-lift system, which is advantageous due to the simpler mechanical system, reduced actuation power and lower maintenance costs. Additionally, the removal of the flap track fairings associated with conventional high-lift systems renders a more efficient aerodynamic configuration. Potentially, these benefits translate to a ~2.25% net reduction in fuel burn for a twinengine,long-range airplane.

15. SUBJECT TERMS

Active flow control; Commercial transport; Common research model; High lift

16. SECURITY CLASSIFICATION OF:			17. LIMITATION OF ABSTRACT	18. NUMBER OF PAGES	19a. NAME OF RESPONSIBLE PERSON
a. REPORT	b. ABSTRACT	c. THIS PAGE			STI Help Desk (email: help@sti.nasa.gov)
U	U	U	UU	37	19b. TELEPHONE NUMBER *(Include area code)* (757) 864-9658